Theory of Deep-Inelastic Lepton-Nucleon Scattering and Lepton Pair Annihilation Processes. II. Deep-Inelastic Electron Scattering*

SIDNEY D. DRELL, DONALD J. LEVY, AND TUNG-MOW YAN
Stanford Linear Accelerator Center, Stanford University, Stanford, California 94305
(Received 1 October 1969)

This is the second in a series of four papers devoted to a theoretical study based on canonical quantum field theory of the deep-inelastic lepton processes. In the present paper we present the detailed calculations leading to the limiting behavior—or the "parton model"—for deep-inelastic electron scattering. It follows from this work that the structure functions depend only on the ratio of energy to momentum transfer $2M\nu/q^2$ as conjectured by Bjorken on general grounds. To accomplish this derivation, it is necessary to introduce a transverse momentum cutoff so that there exists an asymptotic region in which q^2 and $M\nu$ can be made larger than the transverse momenta of all the virtual constituents or "partons" of the proton that are involved. We also derive the ladder approximation for the leading contribution, order by order in the strong interaction and to all orders in the coupling, to the asymptotic behavior of these structure functions with increasing ratio of energy to momentum transfer. Finally, we draw and discuss the experimental implications.

I. INTRODUCTION

THIS is the second in a series of four papers devoted to a theoretical study based on canonical quantum field theory of the deep-inelastic lepton processes including (along with other hadron charges and SU_3 quantum numbers)

$$e^-+p\rightarrow e^-+\text{ anything},$$
$$e^-+e^+\rightarrow p+\text{ anything},$$
$$\nu+p\rightarrow e^-+\text{ anything},$$
$$\bar{\nu}+p\rightarrow e^++\text{ anything}.$$

Electron scattering from hadron targets, and the crossed-channel process of electron-positron annihilation to hadrons, share a singularly attractive feature relative to the various processes of hadrons scattering from hadron targets: The electromagnetic field generated during the electron's scattering is understood if indeed anything is in particle physics. Dirac tells us the transition current of the scattered electron and Maxwell tells us the rest. Therefore, in these processes we are probing the structure of the hadron by an electromagnetic interaction of known form. There is an additional advantage in studying this process and that is its weakness. We can do our theoretical analyses to lowest order in the fine-structure constant $\alpha\approx 1/137$ which is a comfortable expansion parameter for quantitative results. Similarly, to the extent that we have confidence in the $V-A$ theory of weak couplings, the neutrino reactions directly measure the matrix elements of the hadronic weak currents and can, in principle and in practice, be related to the electron processes.

Certain structure functions of the hadron summarize these processes when we detect the energy and momentum of only the one particle indicated explicitly in the above list of reactions and sum over all other final states. This summation over all other hadron states permits us to make headway with the theoretical formalism by making full use of unitarity and completeness. As a result, the distribution of the secondary particles will not be analyzed in detail in our approach. Nevertheless, statements about certain characteristic features of the secondary particle distribution still can be made.

In Paper I,[1,2] we placed primary emphasis on the physical ideas behind the proofs showing how the structure functions of the electron-nucleon scattering in the Bjorken limit of large momentum and energy transfer become universal functions[3] of the ratio of momentum to energy transfer and probe the longitudinal momentum distribution of the "elementary constituents" in the nucleon in an infinite-momentum frame; how the continuation of these structure functions below the inelastic scattering threshold gives predictions for "deep-inelastic" electron-positron annihilation into a proton plus everything else; how the neutrino and antineutrino scattering are related to each other and are closely connected with inelastic electron scattering[4]; and finally how one can understand, at least qualitatively, both the rapid falloff of the electromagnetic nucleon form factors for elastic scattering with increasing momentum transfers and the nonvanishing structure functions for deep-inelastic electron-proton scattering. In this second paper of the series we present the detailed calculations leading to the limiting behavior—or the "parton model"—for deep-inelastic electron scattering. We also derive the ladder approximation as discussed in Ref. 1 for the leading

* Work supported by the U. S. Atomic Energy Commission.

[1] Preliminary results of this work have been reported by S. D. Drell, D. Levy, and T. M. Yan, Phys. Rev. Letters **22**, 744 (1969).

[2] S. D. Drell, D. Levy, and T. M. Yan, Phys. Rev. **187**, 2159 (1969). This paper emphasizes the general ideas, assumptions, and implications and omits detailed calculations. This paper is referred to as Paper I or I.

[3] J. D. Bjorken, Phys. Rev. **179**, 1547 (1969).

[4] R. P. Feynman (unpublished); J. D. Bjorken, in *International School of Physics "Enrico Fermi,"* edited by J. Steinberger (Academic Press Inc., New York, 1968), Course XLI; J. D. Bjorken and E. A. Paschos, Phys. Rev. **185**, 1975 (1969).

contribution, order by order in the strong interaction and to all orders in the coupling, to the asymptotic behavior of these structure functions with increasing ratio of energy to momentum transfer. Finally, we draw and discuss the experimental implications.[5]

The interpretation of our formalism depends heavily on the use of the old-fashioned perturbation theory in an infinite-momentum frame. Therefore, Sec. II is devoted to a brief introduction to rules for calculations in an infinite-momentum frame. Some peculiar phenomena occurring in such a reference frame are discussed. Calculational developments appear in Secs. III and IV and the Appendix, and experimental implications are presented in Sec. V. The analogy between the Bjorken limit and nuclear physics sum rules is also discussed.

II. PROPERTIES OF AN INFINITE-MOMENTUM FRAME AND OLD-FASHIONED PERTURBATION THEORY

As first shown by Bjorken,[3] the infinite-momentum frame of the proton is very useful for studying the structure functions of the proton (hadrons) in the limit of large momentum transfer Q^2 and large energy transfer $M\nu$, with the ratio $w\equiv 2M\nu/Q^2$ fixed. Reasons for looking in this asymptotic kinematic region in search of both a simple, general behavior and interpretation of the structure functions have been discussed elsewhere.[4,6] Feynman, in particular, has emphasized that in a high-energy limit, so that the incident electron and proton are both very relativistic in their c.m. frame, the proton may be viewed as an assemblage of "long-lived" or almost "free" constituents as a result of the time dilation. If the energy transfer from the electron to the proton is also large as viewed in this same frame, the interaction may be treated as a sudden pulse. During the brief duration of this pulse, the constituents—or "partons"—of the proton can be treated as instantaneously free so that an impulse approximation will be valid. The kinematic conditions for this to be a valid approximation are

$$P\to\infty \text{ and } P\gg 2M\nu, Q^2,\quad 2M\nu\to\infty,\ Q^2\to\infty,$$
$$\text{with } w\equiv 2M\nu/Q^2 \text{ finite and } Q^2(w-1)\to\infty.$$

This is the Bjorken limit in which we shall work. Since the validity of the picture of long-lived constituents of the proton that are almost "free" is important to help our intuition, we shall find it useful to work in an infinite-momentum frame in formulating our theory in detail. This section develops the simplifications as well as delicacies of doing field theory in such a frame.

The modern perturbation theory developed by Feynman, Schwinger, and Dyson makes explicit the relativistic covariance of the S matrix at the expense of manifest unitarity by grouping together intermediate states with different numbers of particles and antiparticles. On the other hand, in the so-called old-fashioned perturbation theory, unitarity is more visible but manifest relativistic covariance is lost. Weinberg[7] pointed out that by applying the old-fashioned perturbation theory in a reference frame of infinite total momentum there are substantial calculational simplifications, and a new set of rules appears with properties intermediate between those of Feynman diagrams and those of old-fashioned diagrams. Weinberg found in ϕ^3 theory that the energy denominators become covariant and all intermediate particles must move forward with respect to the total infinite momentum. This latter property prevents creation of particles from the vacuum and greatly simplifies both the interpretation and calculation of the theory.

Unfortunately, as pointed out by Chang and Ma,[8] working in an infinite-momentum frame requires extreme care. They showed, for example, that in ϕ^3 theory vacuum diagrams (diagrams with no external lines) which should vanish according to Weinberg's rule acquire nonvanishing contributions from end points of allowed longitudinal momenta carried by the internal particles. More complications arise in a theory of particles with spin, as we shall illustrate below. However, we should emphasize that despite these unpleasant complications it still can be useful to work in an infinite-momentum frame. This is true if we are dealing with amplitudes in which intermediate states are long lived because of relativistic time dilation. If this is the case, the internal particles are almost real and the violation of energy conservation can be ignored. It is precisely this property which enables us to derive the parton model as sketched in Paper I. It is a property of particular amplitudes and of special kinematic regions and not of the theory in general, however. Therefore, it is not a general simplification for all processes as will become clear in the following.

In the model discussed in Paper I, i.e., the canonical quantum field theory of pseudoscalar pions and nucleons with charge-symmetric γ_5 coupling, the strong dynamics of the pion-nucleon system is described by the interaction Hamiltonian

$$H_I(t)=ig\int d^3x\,\bar\psi(\mathbf{x},t)\gamma_5\boldsymbol{\tau}\psi(\mathbf{x},t)\cdot\boldsymbol{\pi}(\mathbf{x},t)$$
$$=ig\int d^3x[\bar\psi_p\gamma_5\psi_p\pi^0-\bar\psi_n\gamma_5\psi_n\pi^0+\sqrt{2}\bar\psi_p\gamma_5\psi_n\pi^+ +\sqrt{2}\bar\psi_n\gamma_5\psi_p\pi^-], \quad (1)$$

where it is understood that mass renormalization counter terms for the nucleons and the pions are im-

[5] E. Bloom *et al.*, Phys. Rev. Letters **23**, 930 (1969); M. Breidenbach *et al.*, *ibid.* **23**, 935 (1969); W. Albrecht *et al.*, DESY Report No. 69/7 (unpublished).

[6] S. D. Drell, in *Proceedings of the International School of Physics "Ettore Majorana,"* edited by A. Zichichi (Academic Press Inc., New York, to be published), Course 7.

[7] S. Weinberg, Phys. Rev. **150**, 1313 (1966).

[8] S. J. Chang and S. Ma, Phys. Rev. **180**, 1506 (1969).

plicitly included. The electromagnetic current of the hadrons is

$$J_\mu=\bar{\psi}_p\gamma_\mu\psi_p+i\pi^+\overleftrightarrow{\partial}_\mu\pi^-. \tag{2}$$

Equations (1) and (2) do not give a full statement of the theory in our model for the following reason. The value of working in an infinite-momentum frame lies in the simplification of being able to label intermediate particles in a perturbation calculation according to whether they are moving along or in the opposite direction to the infinitely large longitudinal momentum defining the reference frame. Such left-right distinctions are only clear and useful if the transverse momenta at all interaction vertices are small in ratio to the longitudinal momentum. In our theory, this requires us to introduce a transverse momentum cutoff in doing the calculations. This point was discussed more fully in I, and its need and role will become clearer in the following formal developments.

As discussed in I, it will be useful to undress the Heisenberg operators and go into the interaction picture by the usual U-matrix transformation. For example, the Heisenberg current operator $J_\mu(x)$ and the corresponding bare or free current $j_\mu(x)$ are related by

$$J_\mu(x)=U^{-1}(t)j_\mu(x)U(t), \tag{3}$$

where

$$U(t)=\left(\exp\left[-i\int_{-\infty}^{t}d\tau\, H_I(\tau)\right]\right)_+ \tag{4}$$

and j_μ has the same form as (2) written in terms of the free particle in-fields. A basic formula in the old-fashioned perturbation theory which we repeatedly employ is

$$U|a\rangle=(\sqrt{Z_a})\Bigg[|a\rangle+\sum_{n_1}{}'\frac{|n_1\rangle\langle n_1|H_I(0)|a\rangle}{E_a-E_{n_1}+i\epsilon}+\sum_{n_1n_2}{}'\frac{|n_2\rangle\langle n_2|H_I(0)|n_1\rangle\langle n_1|H_I(0)|a\rangle}{(E_a-E_{n_2}+i\epsilon)(E_a-E_{n_1}+i\epsilon)}+\Bigg]\cdots,$$
$$U\equiv U(0) \tag{5}$$

where $\sum'$ indicates the summation over all intermediate states *except* the initial state a; and Z_a, the so-called wave-function renormalization constant, is determined by the normalization condition

$$\langle a'|U^{-1}U|a\rangle=\delta_{aa'}.$$

The states in $|n_1\rangle$, $|n_2\rangle$, etc., are properly symmetrized (antisymmetrized) with respect to identical bosons (fermions) present in these states.

The value of undressing the current in (3) and of assembling the strong-interaction effects into the description of the states lies in the possibility of classifying terms in the infinite-momentum frame. One can separately study the behaviors of the energy denominators in the expansion (5) and of the bare vertices introduced by the interaction matrix elements in the numerators of (5) as well as by $j_\mu(x)$ and identify the leading terms in an infinite-momentum limit. We turn first to the properties of the vertices. To study the properties of the bare vertices in an infinite-momentum frame, it is convenient to use the familiar representation of the Dirac matrices[9]:

$$\gamma^0=\begin{pmatrix}1&0\\0&-1\end{pmatrix},\quad \boldsymbol{\gamma}=\begin{pmatrix}0&\boldsymbol{\sigma}\\-\boldsymbol{\sigma}&0\end{pmatrix},\quad \gamma_5=\begin{pmatrix}0&1\\1&0\end{pmatrix}, \tag{6}$$

where $\boldsymbol{\sigma}=(\sigma_1,\sigma_2,\sigma_3)$ are the 2×2 Pauli spin matrices. The positive (negative) energy solutions of the Dirac equation, denoted by $u_\pm$ ($v_\pm$), are

$$u_\pm(\mathbf{P})=\left(\frac{E+M}{2M}\right)^{1/2}\begin{pmatrix}1\\ \boldsymbol{\sigma}\cdot\mathbf{P}/(E+M)\end{pmatrix}U_\pm, \tag{7}$$

$$v_\pm(\mathbf{P})=\left(\frac{E+M}{2M}\right)^{1/2}\begin{pmatrix}\boldsymbol{\sigma}\cdot\mathbf{P}/(E+M)\\ 1\end{pmatrix}U_\mp, \tag{8}$$

where $+$ and $-$ denote the solutions with the third component of the spin in the rest system pointing up and down, respectively; and $U_\pm$ are two-component Pauli spinors.

In terms of these spinors, the bare γ_5 vertex has the following properties, as the momentum $\mathbf{P}$ tends to infinity along the third axis:

$$\bar{u}(\eta_1\mathbf{P}+\mathbf{k}_{1\perp})\gamma_5 u(\eta_2\mathbf{P}+\mathbf{k}_{2\perp})=\frac{1}{2M}\left(\frac{\eta_1}{\eta_2}\right)^{1/2}U_1^*\left[\boldsymbol{\sigma}\cdot\left(\mathbf{k}_{2\perp}-\frac{\eta_2}{\eta_1}\mathbf{k}_{1\perp}\right)-\sigma_3M\left(1-\frac{\eta_2}{\eta_1}\right)\right]U_2,$$

$$\bar{v}(\eta_1\mathbf{P}+\mathbf{k}_{1\perp})\gamma_5 v(\eta_2\mathbf{P}+\mathbf{k}_{2\perp})=-\frac{1}{2M}\left(\frac{\eta_1}{\eta_2}\right)^{1/2}U_1^*\left[\boldsymbol{\sigma}\cdot\left(\mathbf{k}_{2\perp}-\frac{\eta_2}{\eta_1}\mathbf{k}_{1\perp}\right)-\sigma_3M\left(1-\frac{\eta_2}{\eta_1}\right)\right]U_2,$$

$$\bar{u}(\eta_1\mathbf{P}+\mathbf{k}_{1\perp})\gamma_5 v(\eta_2\mathbf{P}+\mathbf{k}_{2\perp})=\frac{1}{2M}\left(\frac{\eta_1}{\eta_2}\right)^{1/2}U_1^*\left[\left(1+\frac{\eta_2}{\eta_1}\right)M-\sigma_3\boldsymbol{\sigma}\cdot\mathbf{k}_{2\perp}+\sigma_3\boldsymbol{\sigma}\cdot\mathbf{k}_{1\perp}\frac{\eta_2}{\eta_1}\right]U_2, \tag{9}$$

[9] These will be our standard notations. Momentum and energy for a nucleon will be denoted by $\mathbf{P}_i$ and E_i, respectively, those for an antinucleon by $\bar{\mathbf{P}}_i$ and $\bar{E}_i$, respectively, and those for a pion by $\mathbf{k}_i$ and ω_i, respectively. The symbols $\mathbf{P}$ and E_p are reserved for the momentum and energy of the initial nucleon. The nucleon mass and pion mass are M and μ, respectively. Otherwise the notation is that of J. Bjorken and S. Drell, *Relativistic Quantum Mechanics* (McGraw-Hill Book Co., New York, 1964).

$$\bar{u}(\pm\eta_1\mathbf{P}+\mathbf{k}_{1\perp})\gamma_5 u(\mp\eta_2\mathbf{P}+\mathbf{k}_{2\perp})$$
$$=\pm 2(\eta_1\eta_2)^{1/2}PU_1^*\sigma_3 U_2,$$
$$\bar{v}(\pm\eta_1\mathbf{P}+\mathbf{k}_{1\perp})\gamma_5 v(\mp\eta_2\mathbf{P}+\mathbf{k}_{2\perp})$$
$$=\pm 2(\eta_1\eta_2)^{1/2}PU_1^*\sigma_3 U_2,$$
$$\bar{u}(\pm\eta_1\mathbf{P}+\mathbf{k}_{1\perp})\gamma_5 v(\mp\eta_2\mathbf{P}+\mathbf{k}_{2\perp})$$
$$=-2(\eta_1\eta_2)^{1/2}PU_1^*U_2,$$

where η_1, η_2 are positive numbers and $\mathbf{k}_{1\perp}$, $\mathbf{k}_{2\perp}$ are the transverse momenta. Specifically, by infinite-momentum limit we mean that the ratio $k_\perp/P\to 0$ for all $k_\perp$. As mentioned earlier, to enforce this condition it is necessary to impose a cutoff on the theory described by (1) and (2). The important thing to notice in (9) is that when both nucleons (antinucleons or nucleon and antinucleon) move opposite to each other, the vertex becomes infinitely large as P; when they both move forward, the vertex is of order unity. It is this peculiar property that invalidates Weinberg's original argument that all particles must move forward along the direction of the infinite total momentum.

We also need the properties of the bare electromagnetic vertex of the nucleon current in the infinite-momentum frame. They are

$$\bar{u}(\eta_1\mathbf{P}+\mathbf{k}_{1\perp})\begin{Bmatrix}\gamma^0\\ \gamma_3\end{Bmatrix}u(\eta_2\mathbf{P}+\mathbf{k}_{2\perp})=(\eta_1\eta_2)^{1/2}\frac{P}{M}U_1^*U_2$$
$$+\frac{1}{2M}U_1^*\left[\left(\frac{\eta_2}{\eta_1}\right)^{1/2}\sigma_3\boldsymbol{\sigma}\cdot\mathbf{k}_{2\perp}+\left(\frac{\eta_1}{\eta_2}\right)^{1/2}\boldsymbol{\sigma}\cdot\mathbf{k}_{1\perp}\sigma_3\right]U_2,$$
$$\bar{u}(\eta_1\mathbf{P}+\mathbf{k}_{1\perp})\boldsymbol{\gamma}_\perp u(\eta_2\mathbf{P}+\mathbf{k}_{2\perp})=O(1),$$
$$\bar{u}(\pm\eta_1\mathbf{P}+\mathbf{k}_{1\perp})\boldsymbol{\gamma}_\perp\bar{u}(\mp\eta_2\mathbf{P}+\mathbf{k}_{2\perp})$$
$$=\pm(\eta_1\eta_2)^{1/2}\frac{P}{M}U_1^*\boldsymbol{\sigma}_\perp\sigma_3 U_2+O(1),\qquad(10)$$
$$\bar{u}(\pm\eta_1\mathbf{P}+\mathbf{k}_{1\perp})\begin{Bmatrix}\gamma^0\\ \gamma_3\end{Bmatrix}u(\mp\eta_2\mathbf{P}+\mathbf{k}_{2\perp})=O(1),$$
$$\bar{u}(\pm\eta_1\mathbf{P}+\mathbf{k}_{1\perp})\begin{Bmatrix}\gamma^0\\ \gamma_3\end{Bmatrix}v(\mp\eta_2\mathbf{P}+\mathbf{k}_{2\perp})=O(1),$$
$$\bar{u}(\pm\eta_1\mathbf{P}+\mathbf{k}_{1\perp})\boldsymbol{\gamma}_\perp v(\mp\eta_2\mathbf{P}+\mathbf{k}_{2\perp})$$
$$=(\eta_1\eta_2)^{1/2}\frac{P}{M}U_1^*\boldsymbol{\sigma}_\perp U_2+O(1),$$

where $\boldsymbol{\gamma}_\perp$ ($\boldsymbol{\sigma}_\perp$) denotes γ_1 or γ_2 (σ_1 or σ_2). The matrix elements $\bar{v}_1\gamma_\mu v_2$ can be obtained from above by charge conjugation. They are very similar to the corresponding ones $\bar{u}_1\gamma_\mu u_2$. The important thing to notice in (10) is that for the time component and the third component of the nucleon current, the electromagnetic vertex does not have the abnormal property exhibited by the pion-nucleon vertex; namely, the electromagnetic vertex does not introduce any extra power of P when the two nucleons (two antinucleons or nucleon and antinucleon pair) at the vertex have opposite longitudinal momenta. This is also true for the electromagnetic vertices of the pion current. For the transverse components of the nucleon current, the electromagnetic vertex behaves in exactly the opposite way. Therefore, if it is possible to restrict our attention to the time and third component of the electromagnetic current, then Weinberg's argument holds and no particle of negative longitudinal momentum may enter or leave the electromagnetic vertex. For this reason the time component and the third component of J_μ are referred to as "good currents."[10] For processes such as the electron-proton scattering in which the bare current acts only once in the one-photon-exchange approximation it is possible to use only the good currents, and take full advantage of Weinberg's[7] arguments; the contributions from the transverse components can be inferred from covariance requirement.

To illustrate the techniques of calculation in an infinite-momentum frame and simultaneously develop several useful results for the calculation of nucleon structure in Sec. III, we compute to second order in the coupling (1) the wave-function renormalization constants Z_2 and Z_3 for the nucleon and the pion, the mass renormalizations δM and $\delta\mu^2$ for the nucleon and the pion, and the electromagnetic vertex renormalization constant Z_1. The wave-function renormalization constant Z_2 for the proton is defined by

$$|UP\rangle\equiv U|P\rangle$$
$$=(\sqrt{Z_2})\Bigg[|P\rangle+\frac{ig}{(2\pi)^{3/2}}\frac{2M}{(2E_p)^{1/2}}\int\frac{d^3k_1}{(2\omega_1)^{1/2}}\frac{d^3P_1}{(2E_1)^{1/2}}$$
$$\times\delta^3(\mathbf{P}_1+\mathbf{k}_1-\mathbf{P})\frac{\bar{u}_{P_1}\gamma_5 u_P}{E_p-E_1-\omega_1}|P_1k_1\rangle$$
$$+\frac{ig}{(2\pi)^{3/2}}\frac{2M}{(2E_{P_1})^{1/2}}\int\frac{d^3k_1}{(2\omega_1)^{1/2}}\frac{d^3P_1}{(2E_1)^{1/2}}$$
$$\times\frac{d^3\bar{P}_1}{(2\bar{E}_1)^{1/2}}\delta^3(\mathbf{P}_1+\bar{\mathbf{P}}_1+\mathbf{k}_1)\frac{\bar{u}_{P_1}\gamma_5 v_{\bar{P}_1}}{-E_{P_1}-\bar{E}_{P_1}-\omega_1}$$
$$\times|PP_1\bar{P}_1k_1\rangle+O(g^2)+\cdots\Bigg],\qquad(11)$$

where $|P\rangle$ is a one-proton state with momentum $\mathbf{P}$ and energy E_1; and $|P_1k_1\rangle$ is a state with a proton of momentum $\mathbf{P}_1$ and energy E_1 and a neutral pion of momentum $\mathbf{k}_1$ and energy ω_1, etc. The contribution of

[10] We thank Fred Gilman for a discussion of this terminology and its meaning in current algebra.

charged pion can be calculated similarly. We have defined

$$U\equiv U(0). \tag{12}$$

The normalization condition

$$\langle UP|UP'\rangle=\delta^3(\mathbf{P}-\mathbf{P}') \tag{13}$$

determines Z_2. To order g^2, we have

$$Z_2=1-\frac{g^2}{(2\pi)^3}\frac{1}{2E_P}\int\frac{d^3k_1}{2\omega_1}\frac{d^3P_1}{2E_1}\times\delta^3(\mathbf{P}_1+\mathbf{k}_1-\mathbf{P})\frac{(-2)(M^2-PP_1)}{(E_p-E_1-\omega_1)^2}. \tag{14}$$

This is represented graphically by Fig. 1(a), where, as always, the solid lines are for nucleons and dashed ones for pions. The contributions from Figs. 1(b) and 1(c) will be discussed shortly—as will their absence from (14). Let us parametrize the momenta as follows:

$$\mathbf{P}_1=\eta\mathbf{P}+\mathbf{k}_\perp,\quad \mathbf{k}_1=(1-\eta)\mathbf{P}-\mathbf{k}_\perp,\quad \mathbf{k}_\perp\cdot\mathbf{P}=0. \tag{15}$$

In an infinite-momentum frame, $P\to\infty$, we have

$$\begin{aligned}E_P-E_1-\omega_1&=\left(P+\frac{M^2}{2P}\right)-\left(|\eta|P+\frac{k_\perp^2+M^2}{2|\eta|P}\right)\\&\quad-\left(|1-\eta|P+\frac{k_\perp^2+\mu^2}{2|1-\eta|P}\right)\\&=2\eta P+O(1/P),\quad \eta<0\\&=2(\eta-1)P+O(1/P),\quad \eta>1\\&=-\frac{k_\perp^2+M^2(1-\eta)^2+\mu^2\eta}{2\eta(1-\eta)P},\quad 0<\eta<1\end{aligned} \tag{16}$$

and

$$\begin{aligned}-2(M^2-P\cdot P_1)&=4\eta P^2+O(1),\quad \eta<0\\&=\frac{1}{\eta}[k_\perp^2+M^2(1-\eta)^2],\quad \eta>0.\end{aligned} \tag{17}$$

Notice that if all the particles move forward, i.e., both η and $1-\eta$ are positive, the energy denominator $E_p-E_1-\omega_1$ is proportional to $1/P$; on the other hand, it is proportional to P if any of the particles in an intermediate state moves backward, i.e., either η or $1-\eta$ is negative. When there is no possibility of introducing compensating powers of P in the numerator as in ϕ^3 theory, this property enables Weinberg to conclude that all particles must move forward. But from (9) or (17) we see that in a theory of particles with spin such as (1) when one of the nucleons moves backward, the vertex becomes proportional to P. The change of P^2 in *one* energy denominator can be compensated by *two* big vertices. An example of this kind is provided by the calculation of δM below.

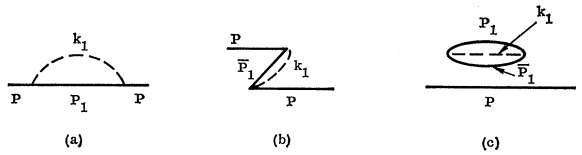

FIG. 1. The three diagrams contributing to the wave-function and mass renormalizations of a nucleon. In the infinite-momentum frame only (a) contributes.

In the case of Z_2 as given by (14), a simple inspection shows that only when the η defined in (15) is between 0 and 1 is the integral nonvanishing as $P\to\infty$. It is this property which makes the infinite-momentum frame so useful; namely, the η integrations are restricted to certain well-defined intervals. Thus

$$Z_{2(\pi^0)}=1-\frac{g^2}{16\pi^2}\int dk_\perp^2\int_0^1 d\eta(1-\eta)\times\frac{k_\perp^2+M^2(1-\eta)^2}{[k_\perp^2+M^2(1-\eta)^2+\mu^2\eta]^2}, \tag{18}$$

where the subscript π^0 indicates the contribution of neutral pions to Z_2. The $k_\perp^2$ integration is logarithmically divergent, as expected from covariant perturbation theory. The corresponding charged-pion contribution to Z_2 can now be written down. It is

$$Z_{2(\pi^+)}=1-\frac{g^2}{8\pi^2}\int dk_\perp^2\int_0^1 d\eta(1-\eta)\times\frac{k_\perp^2+M^2(1-\eta)^2}{[k_\perp^2+M^2(1-\eta)^2+\mu^2\eta]^2}. \tag{19}$$

In the above discussion we have temporarily ignored the contributions of four-particle intermediate states to Z_2 represented by Figs. 1(b) and 1(c). According to the old-fashioned perturbation theory, as in the covariant perturbation theory, we are instructed to omit all disconnected diagrams in calculating a physical amplitude. Thus the contribution of Fig. 1(c) should be excluded. The contribution of Fig. 1(b) is given by an expression similar to (14). Its value is zero as $P\to\infty$, since at least one of the intermediate particles has negative longitudinal momentum. The two large vertices in the numerator are not enough to overcome the large energy denominator squared in (14).

The wave-function renormalization constant for the pion, Z_3, can be computed analogously. The result is

$$\begin{aligned}Z_3&=1-\frac{2g^2}{(2\pi)^3}\frac{1}{2\omega}\int\frac{d^3P}{2E}\frac{4(M^2-P\cdot\bar{P})}{2\bar{E}(\omega-E-\bar{E})^2}\\&=1-\frac{g^2}{4\pi^2}\int dk_\perp^2\int_0^1 d\eta\frac{k_\perp^2+M^2}{[k_\perp^2+M^2-\mu^2\eta(1-\eta)]^2}.\end{aligned} \tag{20}$$

The diagrams contributing to Z_3 are shown in Fig. 2.

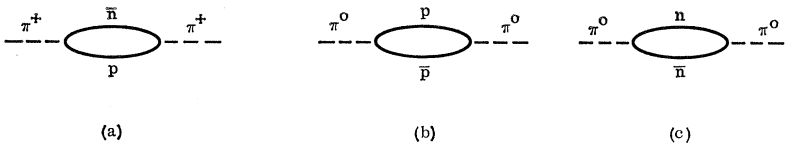

FIG. 2. Diagrams contributing to the wave-function and mass renormalizations of a pion.

We now compute the contribution to Z_1 from one-π^0 exchange. The contribution from charged-pion exchange will be included later. In general, there are six time-ordered diagrams as shown in Fig. 3 contributing to the vertex corrections. (*Note added in proof.* We omit additional graphs in which the electromagnetic vertex lies on an external leg. These all vanish as $P\to\infty$. We thank D. Soper for calling this point to our attention.) Equation (3) gives

$$\langle P|J_\mu(0)|P'\rangle=\langle UP|j_\mu(0)|UP'\rangle. \tag{21}$$

To compute Z_1 set $q=P'-P=0$. Using (9), (10), and (21) one concludes that for good currents only Fig. 3(a) contributes.

The situation is different for transverse components of the current to which other diagrams also contribute. For example, in Figs. 3(b) and 3(e), if we write

$$\begin{aligned}\mathbf{P}_1&=-\bar{\mathbf{P}}_1=\eta\mathbf{P}+\mathbf{k}_\perp,\\ \mathbf{k}_1&=(1-\eta)\mathbf{P}-\mathbf{k}_\perp,\end{aligned} \tag{22}$$

then the region $0<\eta<1$, where the antiproton moves backward, contributes. Although one of the energy denominators in this region is of order P, instead of $1/P$, it is compensated by the powers of P introduced at the large strong vertex and at the large bare electromagnetic vertex of a transverse component.

Figures 3(c), 3(d), and 3(f) never contribute since *both* energy denominators in these diagrams are of order P. This is a general rule. *By simple power counting, two big vertices are always required to compensate for one big energy denominator.* Therefore, a particle created with negative longitudinal momentum must either be absorbed or change its sign of longitudinal momentum at the next vertex. It cannot traverse beyond a vertex without being disturbed. This result eliminates many otherwise possible diagrams in an infinite-momentum frame, and it will be repeatedly utilized without explicit reference in our subsequent discussion.

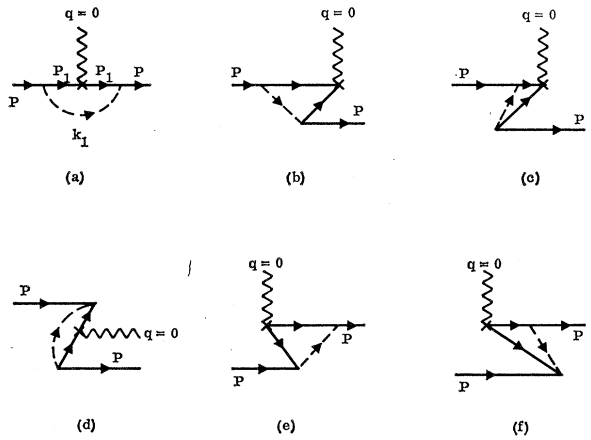

FIG. 3. Second-order corrections to the nucleon electromagnetic vertex from the proton current.

Relativistic covariance of the theory allows us to compute Z_1 by restricting J_μ to good components ($\mu=0$ or 3); then only Fig. 3(a) contributes. Obviously, one can compute Z_1 using the transverse components of J_μ. But then extreme care and extra labor are needed. From the definition of Z_1 and using good currents, we have

$$\begin{aligned}&\bar{u}_p\gamma_\mu u_p(Z_1^{-1}-1)\\ &\quad=\bar{u}_p\frac{P_\mu}{M}u_p(Z_1^{-1}-1)\\ &\quad=\frac{g^2}{(2\pi)^3}\int\frac{d^3k_1}{2\omega_1}\frac{\bar{u}_p(M-\gamma P_1)\gamma_\mu(M-\gamma P_1)u_p}{(2E_1)^2(E_p-E_1-\omega_1)^2}\\ &\quad=\frac{g^2}{(2\pi)^3}\frac{1}{M}\int\frac{d^3k_1}{2\omega_1}\frac{(-2)(M^2-P\cdot P_1)\bar{u}_pP_{1\mu}u_p}{(2E_1)^2(E_p-E_1-\omega_1)^2}.\end{aligned} \tag{23}$$

Using the parametrization (15) and $P_{1\mu}=\eta P_\mu$ for $\mu=0$ or 3, we obtain, to order g^2,

$$Z_{1(\pi^0)}=1-\frac{g^2}{16\pi^2}\int dk_\perp^2\int_0^1 d\eta(1-\eta)\times\frac{k_\perp^2+M^2(1-\eta)^2}{[k_\perp^2+M^2(1-\eta)^2+\mu^2\eta]^2}. \tag{24}$$

In comparison with (18) we find

$$Z_{1(\pi^0)}=Z_{2(\pi^0)}, \tag{25}$$

provided the cutoffs for the $k_\perp^2$ integration in both expressions are identical. This identity of renormalization constants is required by the Ward identity.

Contributions to Z_1 due to exchange of a charged pion also include six diagrams in general as shown in Fig. 4.

A simple power counting shows that only Fig. 4(a) contributes for any of the four components of J_μ. Calculations similar to (23) give

$$\begin{aligned}&\bar{u}_p\frac{P_\mu}{M}u_p(Z_1^{-1}-1)\\ &\quad=\frac{g^2}{(2\pi)^3}\int\frac{d^3k_1}{2\omega_1}\frac{(-2)(M^2-P\cdot P_1)}{(2E_1)(E_p-E_1-\omega_1)^2}\frac{k_{1\mu}}{\omega_1}\bar{u}_pu_p.\end{aligned} \tag{26}$$

The parametrization (15) gives for $\mu=0$ or 3, to order g^2,

$$Z_{1(\pi^+)}=1-\frac{g^2}{8\pi^2}\int dk_\perp{}^2\int_0^1 d\eta(1-\eta)\times\frac{k_\perp{}^2+M^2(1-\eta)^2}{[k_\perp{}^2+M^2(1-\eta)^2+\mu^2\eta]^2}, \quad (27)$$

which shows, again in accord with the Ward identity,

$$Z_{1(\pi^+)}=Z_{2(\pi^+)}. \quad (28)$$

If one chooses $\mu=1$, 2, then (26) is a trivial identity. The left-hand side of (26) vanishes because P_μ has no transverse component and the right-hand side vanishes after symmetrical integration of k.

The second-order mass renormalization of a nucleon, δM, can be computed by the familiar formula for second-order energy-level shift in the old-fashioned perturbation theory:

$$\delta E_n=\sum_m{}'\frac{|\langle n|H_I(0)|m\rangle|^2}{E_n-E_m}, \quad (29)$$

where the summation $\sum'$ excludes $m=n$. Equation (29) and the mass-shell relation $E_p{}^2=P^2+M^2$ give

$$\delta M=\frac{E_p}{M}\sum_n{}'\frac{|\langle P|H_I(0)|n\rangle|^2}{E_p-E_n}. \quad (30)$$

The charged-pion contribution will be ignored since it can be obtained trivially from the neutral-pion contribution.

We reproduce this calculation to illustrate an example in which extra care must be taken in dealing with the extremes of the $d\eta$ integrations. To order g^2, there are three contributions corresponding to the three diagrams in Fig. 1. Again the disconnected diagram Fig. 1(c) will be omitted. The contributions of Figs. 1(a) and 1(b), denoted by δM_a and δM_b, respectively, are

$$\delta M_a=\frac{g^2}{(2\pi)^3}\frac{1}{M}\int\frac{d^3k_1}{2\omega_1}\frac{-(M^2-P\cdot P_1)}{2E_1(E_p-E_1-\omega_1)},$$
$$\delta M_b=\frac{g^2}{(2\pi)^3}\frac{1}{M}\int\frac{d^3k_1}{2\omega_1}\frac{(M^2+P\cdot\bar{P}_1)}{2\bar{E}_1(E_p+\bar{E}_1+\omega_1)}, \quad (31)$$

where the momentum labels are indicated in Fig. 1. For δM_a using the parametrization (15) and taking the limit $P\to\infty$ we find that there are two regions of η contributing, $0<\eta<1$ and $\eta<0$, corresponding to the intermediate nucleon moving forward and backward. Thus

$$\delta M_a=\delta M_a{}^{(1)}+\delta M_a{}^{(2)}+\delta M_a{}^{(3)}, \quad (32)$$

$$\delta M_a{}^{(1)}=-\frac{g^2}{16\pi^2}\frac{1}{2M}\int dk_\perp{}^2\int_\epsilon^1\frac{d\eta}{\eta}\frac{k_\perp{}^2+M^2(1-\eta)^2}{k_\perp{}^2+M^2(1-\eta)^2+\mu^2\eta}, \quad (33)$$

$$\delta M_a{}^{(2)}=\frac{g^2}{16\pi^2}\frac{1}{2M}\int dk_\perp{}^2\int_{-\infty}^{-\epsilon}d\eta\frac{1}{\eta(1-\eta)}. \quad (34)$$

Since the resulting η integrations diverge at $\eta=0$, a small cutoff ϵ is given to both sides of $\eta=0$. The contribution from the infinitesimal region $-\epsilon<\eta<\epsilon$ is denoted by $\delta M_a{}^{(3)}$. For δM_b the following parametrization for the momenta is used:

$$\bar{\mathbf{P}}_1=-\eta\mathbf{P}-\mathbf{k}_\perp,\quad \mathbf{k}_1=-(1-\eta)\mathbf{P}+\mathbf{k}_\perp,\quad \mathbf{k}_\perp\cdot\mathbf{P}=0. \quad (35)$$

In the limit $P\to\infty$, we find

$$\delta M_b=\delta M_b{}^{(1)}+\delta M_b{}^{(2)}+\delta M_b{}^{(3)}, \quad (36)$$

$$\delta M_b{}^{(1)}=\frac{g^2}{16\pi^2}\frac{1}{2M}\int dk_\perp{}^2\int_0^{1-\epsilon}\frac{d\eta}{1-\eta}, \quad (37)$$

$$\delta M_b{}^{(2)}=-\frac{g^2}{16\pi^2}\frac{1}{2M}\int dk_\perp{}^2\int_{1+\epsilon}^{\infty}\frac{d\eta}{\eta(1-\eta)}. \quad (38)$$

Again the resulting η integrations diverge at $\eta=1$. For simplicity and anticipating the procedure to be correct, the same cutoff ϵ as in δM_a is given to both sides of $\eta=1$ here. The contribution from the infinitesimal region $1-\epsilon<\eta<1+\epsilon$ is denoted by $\delta M_b{}^{(3)}$. Collecting terms, we obtain

$$\delta M=\frac{g^2}{16\pi^2}\frac{\mu^2}{2M}\int dk_\perp{}^2\int_0^1 d\eta\frac{1}{k_\perp{}^2+M^2(1-\eta)^2+\mu^2\eta}+\delta M_a{}^{(3)}+\delta M_b{}^{(3)}. \quad (39)$$

Since the η integration in the first term converges now,

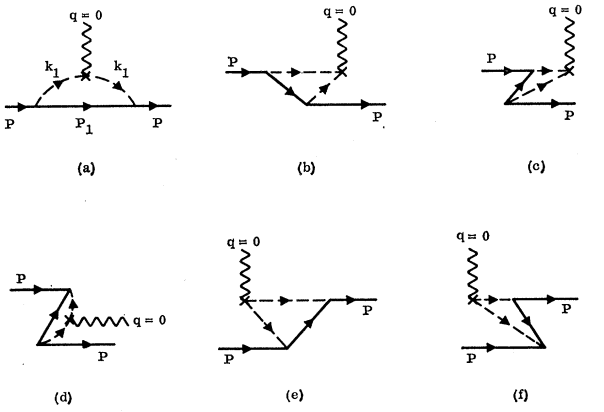

FIG. 4. Second-order corrections to the nucleon electromagnetic vertex from the pion current.

the cutoff ϵ is unnecessary and therefore is set to zero. It is interesting to notice that if $\delta M_2^{(3)}$ and $\delta M_b^{(3)}$ are ignored, δM vanishes with μ^2, in conflict with the known result in covariant perturbation theory. Thus, the main contribution to δM must come from the infinitesimal regions of η, i.e., $\delta M_a^{(3)}$ and $\delta M_b^{(3)}$. We verify this statement by explicit calculation. Using (15), we have for $\eta \sim 0$

$$\begin{aligned} -(M^2-P\cdot P_1) &\approx -P[\eta P-(\eta^2P^2+k_\perp^2+M^2)^{1/2}], \\ E_p-E_1-\omega_1 &\approx \eta P-(\eta^2P^2+k_\perp^2+M^2)^{1/2}, \end{aligned} \tag{40}$$

and

$$\delta M_a^{(3)} = -\frac{g^2}{16\pi^2}\frac{1}{2M} \times \int dk_\perp^2 \int_{-\epsilon}^{\epsilon} \frac{d\eta}{[\eta^2+(k^2+M^2)/P^2]^{1/2}}, \tag{41}$$

i.e.,

$$\delta M_a^{(3)} = \frac{-g^2}{16\pi^2}\frac{1}{2M}\int dk_\perp^2 \ln\frac{(P\epsilon)^2}{k_\perp^2+M^2}. \tag{42}$$

Similarly, using (35), we obtain

$$\delta M_b^{(3)} = \frac{g^2}{16\pi^2}\frac{1}{2M}\int dk_\perp^2 \ln\frac{(P\epsilon)^2}{k_\perp^2+\mu^2}. \tag{43}$$

Observe that $\delta M_a^{(3)}$ and $\delta M_b^{(3)}$ separately diverge as $P\to\infty$ or $\epsilon\to 0$. The sum of the two, however, becomes independent of both P and ϵ.

$$\delta M_a^{(3)}+\delta M_b^{(3)} = \frac{g^2}{16\pi^2}\frac{1}{2M}\int dk_\perp^2 \ln\frac{k_\perp^2+M^2}{k_\perp^2+\mu^2}. \tag{44}$$

Finally, δM can be written in the parametric form

$$\delta M = \frac{g^2}{16\pi^2}\int dk_\perp^2 \int_0^1 d\eta \frac{M(1-\eta)}{k_\perp^2+M^2(1-\eta)^2+\mu^2}, \tag{45}$$

which can be verified to be in agreement with covariant perturbation calculation.

The mass renormalization of a pion, $\delta\mu^2$, can be computed similarly. We record here only the contribution of the diagram of Fig. 2(b) in which both intermediate particles move forward. This contribution will be referred to later. It is

$$(\delta\mu^2)_{2b} = \frac{2g^2}{(2\pi)^3}\int \frac{d^3P_1}{2E_1}\frac{\mathrm{Tr}\{(M-\gamma P_1)(M-\gamma\bar{P}_1)\}}{2\bar{E}_1(\omega_1-E_1-\bar{E}_1)}. \tag{46}$$

In this section we have seen in simple examples some of the subtleties in the infinite-momentum-frame calculations. Sufficient care must be exercised if calculations are performed in such a reference frame. As a general rule, there is need to use extra care in handling a diagram if, and only if, after taking the limit $P\to\infty$ and before doing any integration, the diagram diverges at the end points of the η integrations.

III. DERIVATION OF PARTON MODEL FOR DEEP-INELASTIC ELECTRON SCATTERING

We turn now to the physical process of inelastic electron-nucleon scattering. We are interested in the two structure functions summarizing hadron dynamics as probed by experiments that detect only the four-momentum of the outgoing electron and sum over all hadron final states compatible with the over-all conservation laws. These functions are labeled W_1 and W_2 and defined as earlier by[11]

$$\begin{aligned} W_{\mu\nu} &= 4\pi^2\frac{E_p}{M}\int (dx)e^{+iq\cdot x}\langle P|J_\mu(x)J_\nu(0)|P\rangle \\ &= 4\pi^2\frac{E_p}{M}\sum_n \langle P|J_\mu(0)|n\rangle\langle nJ_\nu(0)|P\rangle \\ &\qquad \times(2\pi)^4\delta^4(q+P-P_n) \\ &= -\left(g_{\mu\nu}-\frac{q_\mu q_\nu}{q^2}\right)W_1(q^2,\nu)+\frac{1}{M^2}\left(P_\mu-\frac{P\cdot q}{q^2}q_\mu\right) \\ &\qquad \times\left(P_\nu-\frac{P\cdot q}{q^2}q_\nu\right)W_2(q^2,\nu), \end{aligned} \tag{47}$$

where $|P\rangle$ is a one-nucleon state with four-momentum P_μ, q_μ is the four-momentum of the virtual photon, $q^2=-Q^2<0$ is the mass squared of the virtual photon, and $M\nu=q\cdot P$ is the energy transfer to the nucleon in the laboratory system; $w\equiv 2M\nu/Q^2$. An average over the nucleon spin is understood in the definition of $W_{\mu\nu}$. Since $(q+P)^2\geq M^2$, we must have $1<w<\infty$. If $w=1$, only the elastic process $e+P\to e'+P'$ contributes to (47). However, as long as $w-1\neq 0$, the invariant mass of the final hadrons, $(q+P)^2=Q^2(w-1)+M^2$, becomes very large as Q^2, $M\nu\to\infty$ with w fixed. Therefore all possible inelastic channels contribute to (47) in this deep-inelastic region. Since we are interested in the deep-inelastic continuum and not the resonance excitations, we shall always require $2M\nu-Q^2=Q^2(w-1)\gg M^2$ in the following.

We perform our calculations in the infinite-momentum c.m. frame of the electron and nucleon $P\to\infty$, where P is the energy of the incident electron and proton, and the components of the momentum transfer are

$$\begin{aligned} q^0 &= \frac{2M\nu-Q^2}{4P}, \quad q_3 = \frac{-2M\nu-Q^2}{4P}, \\ |\mathbf{q}_\perp| &= \sqrt{(Q^2)}+O(1/P^2), \end{aligned} \tag{48}$$

with the nucleon momentum $\mathbf{P}$ along the 3 axis. We now

[11] S. D. Drell and J. D. Walecka, Ann. Phys. (N. Y.) **28**, 18 (1964).

undress the current operator with the aid of (3) and rewrite (47) as follows:

$$W_{\mu\nu}=4\pi^2\frac{E_p}{M}\sum\langle UP|j_\mu(0)U|n\rangle\langle n|U^{-1}j_\nu(0)|UP\rangle \times(2\pi)^4\delta^4(q+P-P_n). \quad (49)$$

In approaching the task of evaluating (49), we recall several general features of old-fashioned perturbation theory that simplify our task. First the spatial momentum is conserved at each vertex and the energy is not. This is already clear in (11), where the momentum δ functions result from the volume integral in the interaction (1), whereas the energy denominators arise from the time integral from $\tau=-\infty$ to $\tau=0$ in the U matrix in constructing (5). Since the currents and fields have been undressed by the U transformation, *free* bare particles are being created and destroyed at the vertices and, although not on their energy shells, they are on their mass shells—i.e., $\omega_i^2=k_i^2+\mu^2$ and $E_{p_i}^2=P_i^2+M^2$ everywhere. Furthermore, we understand that all disconnected diagrams are excluded[12] in our discussions and calculations and in particular in the expansion of (49).

Many diagrams in the expansion of (49) vanish in an infinite-momentum frame which otherwise contribute. First we recall the general rule derived in Sec. II that a large or bad energy denominator requires two large vertices to overcome it. This rule eliminates diagrams of the type shown in Fig. 5 if they appear in the expansion of $|UP\rangle$ or $U|n\rangle$. In these diagrams either a pion created from the vacuum carries a negative longitudinal momentum or a nucleon (antinucleon) with negative longitudinal momentum traverses across a vertex without being annihilated or converted into a particle with positive longitudinal momentum.

We may also restrict our attention to good components of the current j_μ in (49), i.e., $\mu=0$ or 3, since the covariant structure (47) allows us to infer W_1 and W_2 from W_{00} and W_{33}. In the infinite-momentum frame where q is almost transverse, as indicated in (48), the electromagnetic current does not alter significantly ($\sim 1/P$ relative to P) the conservation of longitudinal momentum of the hadrons at the electromagnetic vertex. Then the discussion in the preceding paragraph shows also that an electromagnetic vertex cannot occur in between two strong vertices where the intermediate state contains particles with negative longitudinal momentum. Also, a charged particle and its antiparticle cannot annihilate at the electromagnetic vertex since

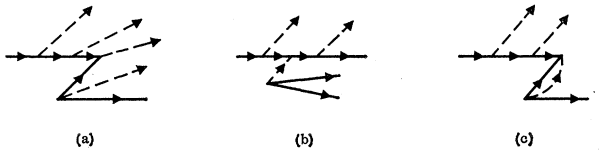

FIG. 5. Examples of parts of diagrams which cannot appear in the infinite-momentum frame.

they must have longitudinal momenta opposite to each other in which case the electromagnetic vertex is reduced by $1/P$. For these diagrams, the powers of P introduced by the large energy denominators are more than can be overcome by the large vertices in the numerator. Therefore, diagrams as illustrated in Fig. 6, where the electromagnetic current operates at the vertex marked ×, are also eliminated in the infinite-momentum frame we are working in.

We can also infer from these discussions the important conclusions that all the *final* particles in the expansion of $|UP\rangle$, i.e., all particles existing at the instant of the current interaction as given by (11), and the *real* particles present in the final states $|n\rangle$ must have positive longitudinal momenta. Suppose there is one particle in $|UP\rangle$ moving with negative longitudinal momentum. This particle may scatter or be annihilated by the electromagnetic current or may not even interact with it at all. The electromagnetic vertex will not change the direction of the longitudinal momentum of this particular particle if it does not interact with the current or if it scatters from the current, since the virtual photon has to order $1/P$ only transverse momentum. As a result in these cases, such a particle appears in $U|n\rangle$ if it is present in $|UP\rangle$ and this thereby introduces at least *two* large energy denominators and at most two big vertices. Since the two denominators reduce the contribution by $(P^2)^2$ and two big vertices enhance it by at most P^2, this cannot contribute to leading order.

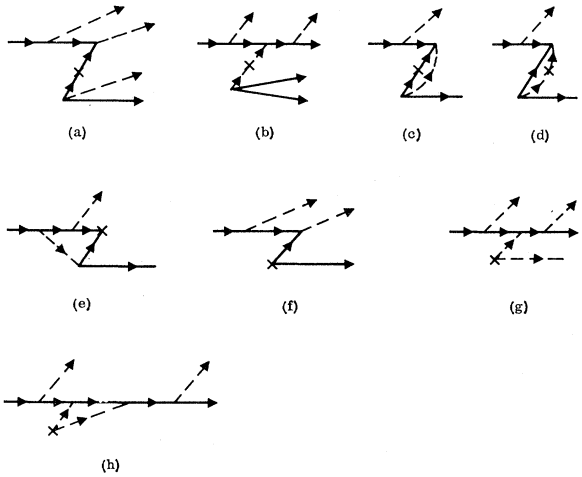

FIG. 6. Examples of electromagnetic vertices which do not contribute in the infinite-momentum frame specified by Eq. (48) when only good currents are used.

[12] There are particular diagrams in which particles created from the vacuum at a single vertex may all appear as final real particles. Bubbles with no external lines may also be part of a diagram. Furthermore, a counter term should be introduced into H_I of (1) to account for the energy shift of the vacuum state in the presence of interaction. It is well known that contributions of these three classes of diagrams to any physical quantity cancel among themselves, and therefore as a whole they make no effect on the final answer.

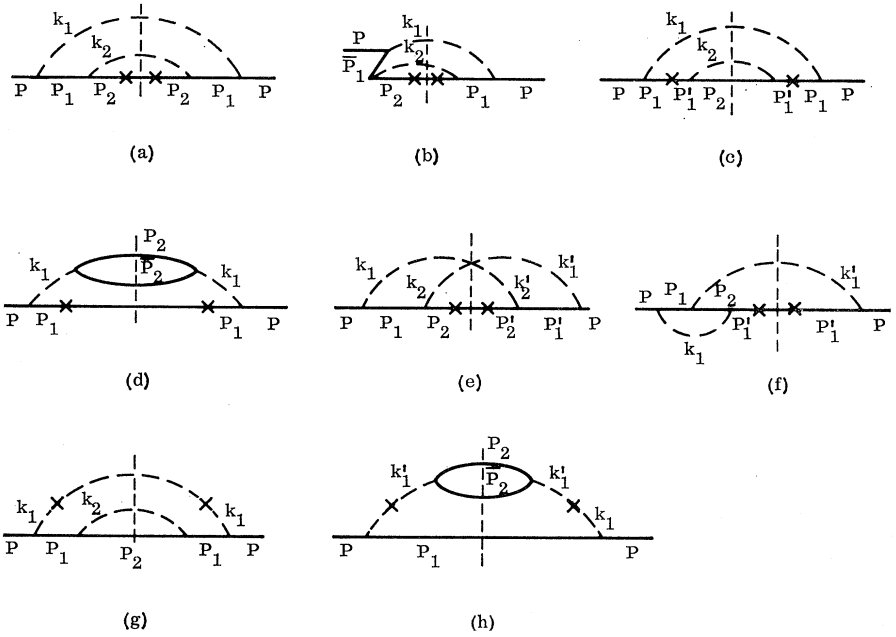

FIG. 7. Typical examples of diagrams which appear in the perturbation expansion of $Z_{\mu\nu}$.

The case in which this particle with negative longitudinal momentum is annihilated, together with its antiparticle with positive momentum, by the current is ruled out to leading order as discussed in the preceding paragraph. Finally, suppose there is a particle in the final state $|n\rangle$ moving with negative longitudinal momentum. However, this possibility is ruled out by the energy-conserving delta function in (49) since, to leading order as $P\to\infty$, we must have that $E_n\to E_p\approx P$.[13]

In the Bjorken limit of large Q^2 and $M\nu$, (49) greatly simplifies. This simplification is intimately related to our fundamental assumption made in Paper I that there exists an asymptotic region in which Q^2 can be made greater than the transverse momenta of all the particles involved, i.e., of the pions and nucleons that are the (virtual) constituents or partons of the nucleon. Such an assumption is consistent with present high-energy data that strongly indicate that transverse momenta of the final particles are indeed very limited in magnitude. In our analysis we suppress large transverse momentum transfers by simply inserting a transverse momentum cutoff at every strong vertex as commented earlier.

The cutoff procedure employed in our formalism is illustrated by the following examples of typical diagrams in Fig. 7 contributing to (49). Along with these examples we also illustrate how the allowed values of the longitudinal momenta are determined. Consider the time-ordered diagrams in Fig. 7. The vertical dashed lines intersect the real physical final states produced from the initial proton by the current which interacts at a vertex marked ✕. The momenta for the nucleons and pions are indicated. For Figs. 7(a) and 7(g) the momenta will be parametrized as follows:

$$\begin{aligned}&\mathbf{P}_1=\eta_1\mathbf{P}+\mathbf{k}_{1\perp},\quad \mathbf{k}_1=(1-\eta_1)\mathbf{P}-\mathbf{k}_{1\perp},\\ &\qquad\qquad 0<\eta_1<1,\quad \mathbf{k}_{1\perp}\cdot\mathbf{P}=0;\\ &\mathbf{P}_2=\eta_2\mathbf{P}_1+\mathbf{k}_{2\perp},\quad \mathbf{k}_2=(1-\eta_2)\mathbf{P}_1-\mathbf{k}_{2\perp},\\ &\qquad\qquad 0<\eta_2<1,\quad \mathbf{k}_{2\perp}\cdot\mathbf{P}_1=0.\end{aligned}\tag{50}$$

For Fig. 7(b) they are parametrized as follows:

$$\begin{aligned}&\mathbf{P}_1=-\bar{\mathbf{P}}_1=\eta_1\mathbf{P}+\mathbf{k}_{1\perp},\quad \mathbf{k}_1=(1-\eta_1)\mathbf{P}-\mathbf{k}_{1\perp},\\ &\qquad\qquad 0<\eta_1<1,\quad \mathbf{k}_{1\perp}\cdot\mathbf{P}=0;\\ &\mathbf{P}_2=\eta_2\mathbf{P}_1+\mathbf{k}_{2\perp},\quad \mathbf{k}_2=(1-\eta_2)\mathbf{P}_1-\mathbf{k}_{2\perp},\\ &\qquad\qquad 0<\eta_2<1,\quad \mathbf{k}_{2\perp}\cdot\mathbf{P}_1=0.\end{aligned}\tag{51}$$

For Fig. 7(c) the parametrizations are

$$\begin{aligned}&\mathbf{P}_1=\eta_1\mathbf{P}+\mathbf{k}_{1\perp},\quad \mathbf{k}_1=(1-\eta_1)\mathbf{P}-\mathbf{k}_{1\perp},\\ &\qquad\qquad 0<\eta_1<1,\quad \mathbf{k}_{1\perp}\cdot\mathbf{P}=0;\\ &\mathbf{P}_1'=\mathbf{P}_1+\mathbf{q},\\ &\mathbf{P}_2=\eta_2\mathbf{P}_1'+\mathbf{k}_{2\perp},\quad \mathbf{k}_2=(1-\eta_2)\mathbf{P}_1'-\mathbf{k}_{2\perp},\\ &\qquad\qquad 0<\eta_2<1,\quad \mathbf{k}_{2\perp}\cdot\mathbf{P}_1'=0.\end{aligned}\tag{52}$$

For Figs. 7(d) and 7(h) we adopt the parametrizations

$$\begin{aligned}&\mathbf{P}_1=\eta_1\mathbf{P}+\mathbf{k}_{1\perp},\quad \mathbf{k}_1=(1-\eta_1)\mathbf{P}-\mathbf{k}_{1\perp},\\ &\qquad\qquad 0<\eta_1<1,\quad \mathbf{k}_{1\perp}\cdot\mathbf{P}=0;\\ &\mathbf{k}_1'=\mathbf{k}_1+\mathbf{q},\\ &\mathbf{P}_2=\eta_2\mathbf{k}_1'+\mathbf{k}_{2\perp},\quad \bar{\mathbf{P}}_2=(1-\eta_2)\mathbf{k}_1'-\mathbf{k}_{2\perp},\\ &\qquad\qquad 0<\eta_2<1,\quad \mathbf{k}_{2\perp}\cdot\mathbf{k}_1'=0.\end{aligned}\tag{53}$$

The allowed regions for the η's given above are determined by our observation that all the final particles in $|UP\rangle$ and particles present in the final states $|n\rangle$ must have positive longitudinal momenta.

[13] Detailed calculations verify that the extreme end regions $\eta\sim0$ and $\eta\sim1$ contribute negligibly. Although we can give no general proof of this, it can be explicitly verified for specific cases.

Our cutoff procedure states simply that the squared length of the transverse momenta $k_{i\perp}$'s of each vertex as defined above never exceed a maximum value $k_{\perp\,\max}{}^2$. Notice that the "transverse momenta" k_i's are not defined with respect to the fixed direction given by P. This definition of $k_{i\perp}$'s and the cutoff procedure just described are reasonable since the cutoff, a property of a vertex, should depend only on the characteristics at the given vertex and should be independent of what has happened preceding it. The simple sharp-cutoff procedure may be replaced by a more elaborate smooth one such as a form factor. Such a procedure, however, will not change the basic features of the general formalism but only detailed numerical predictions of our model. Since our detailed predictions of this kind, as will be shown in Sec. IV, are insensitive to the precise cutoff, we are justified to adopt such a simple cutoff procedure. *In the present context the entire and sole use of the cutoff is to make all integrals over intermediate particle momenta finite as we let* $Q^2\to\infty$, *so that we can classify leading terms in a hierarchy simply according to numbers of powers of* Q^2 *in the numerator minus the number in the denominator.*

Return to the other diagrams in Fig. 7. Suppose that, for Fig. 7(e), $\mathbf{P}_1$, $\mathbf{k}_1$, $\mathbf{P}_2$, and $\mathbf{k}_2$ are parametrized as (50) and $\mathbf{P}_1'$, $\mathbf{k}_1'$, $\mathbf{P}_2'$, and $\mathbf{k}_2'$ are to be determined by momentum conservation. Because of the sharp finite cutoff for $\mathbf{k}_{i\perp}$ and $\mathbf{k}_{i\perp}'$, the relations between primed and unprimed quantities are very complicated. Again we are not interested in the precise numerical values but only in a classification according to leading powers of Q^2. For simplicity, in these diagrams with crossed lines we will use a slightly different parametrization. For instance, the momenta in Fig. 7(e) will be parametrized as follows:

$$\begin{aligned}
&\mathbf{P}_1=\eta_1\mathbf{P}+\mathbf{k}_{1\perp}, \quad \mathbf{k}_1=(1-\eta_1)\mathbf{P}-\mathbf{k}_{1\perp}=\mathbf{k}_2', \\
&\qquad\qquad 0<\eta_1<1, \quad \mathbf{k}_{1\perp}\cdot\mathbf{P}=0; \\
&\mathbf{P}_1'=\eta_1'\mathbf{P}+\mathbf{k}_{1\perp}', \quad \mathbf{k}_1'=(1-\eta_1')\mathbf{P}-\mathbf{k}_{1\perp}'=\mathbf{k}_2, \\
&\qquad\qquad 0<\eta_1'<1, \quad \mathbf{k}_{1\perp}'\cdot\mathbf{P}=0; \\
&\mathbf{P}_2=(\eta_1+\eta_1'-1)\mathbf{P}+(\mathbf{k}_{1\perp}+\mathbf{k}_{1\perp}')=\mathbf{P}_2', \\
&\qquad\qquad 0<\eta_1+\eta_1'-1<1
\end{aligned} \tag{54}$$

where the allowed regions for η_1 and η_1' are such that all the final real particles have positive longitudinal momenta. The parametrization (54) implicitly assumes the complete overlap between $\mathbf{k}_1$, $\mathbf{k}_2$ and $\mathbf{k}_1'$, $\mathbf{k}_2'$, although this is not strictly true because the cutoff for the transverse momenta is finite. This particular parametrization has the advantage that it is symmetrical with respect to the two halves of the diagram. In the same spirit we parametrize the momenta in Fig. 7(f) as given by (54), but the allowed regions for η_1 are different. Since $\mathbf{k}_1'$ is the momentum of a final real particle, $1-\eta_1'$ can vary between 0 and 1. The nucleon with momentum P_2 is virtual and therefore may have positive or negative longitudinal momentum,

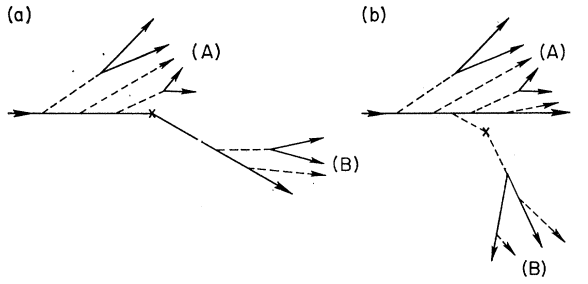

FIG. 8. Diagram illustrating pions and nucleons moving in well-separated and identified groups along the directions $\mathbf{P}$ and $(1/w)\mathbf{P}+\mathbf{q}$. This illustrates the effect of the transverse momentum cutoff and the meaning of an asymptotic region in our model.

corresponding, respectively, to the two allowed regions of η_1: $1>\eta_1>(1-\eta_1')$ and $(1-\eta_1')>\eta_1>0$.

We now turn to the simplifications introduced in our model of (1) with a maximum transverse momentum cutoff when we go to the Bjorken limit. In this limit, certain classes of diagrams in (49) vanish. To make this simplification apparent, we consider the time-ordered sequence of events in the old-fashioned perturbation-theory description of a scattering process as represented by the matrix element $\langle UP|j_\mu(0)U|n\rangle$. Before the bare current $j_\mu(0)$ operates, $|UP\rangle$ describes emission and reabsorption of pions and nucleon-antinucleon pairs. The bare electromagnetic current scatters one of the charged constituents in $|UP\rangle$ and imparts to it a very large transverse momentum $|\mathbf{q}_\perp|\approx\sqrt{(Q^2)}$. The unscattered constituents in $|UP\rangle$ keep moving and emit and reabsorb pions and nucleon-antinucleon pairs. They form a group of particles moving very close to each other along the direction $\mathbf{P}$ as large transverse momenta are suppressed by the cut-off vertices. The scattered charged constituent also emits and reabsorbs pions and nucleon-antinucleon pairs. Analogously these form a second group of particles moving close to each other but along a direction which deviates in transverse momentum by $\mathbf{q}_\perp$ from the first group. These two groups of particles, denoted by (A) and (B), are illustrated in Fig. 8. As $\mathbf{q}_\perp\to\infty$, the cut-off strong vertices prevent any particle emitted by group (A) from being absorbed by group (B) and vice versa. Consequently, there is no interaction between the two well-separated groups of particles. It is then obvious that diagrams corresponding to electromagnetic vertex corrections (Fig. 9) or more complicated diagrams describing interactions between the two groups of particles (Fig. 10) vanish in the limit $\mathbf{q}_\perp\to\infty$. It is equally obvious that coherent interference between the two matrix elements $\langle UP|j_\mu(0)U|n\rangle$ and $\langle n|U^{-1}j_\nu(0)|UP\rangle$ in (49) is impossible unless they both produce the identical sets of well-separated particle groups (A), (B) and (A'), (B'). As a result diagrams of the type given in Fig. 11 vanish as $\mathbf{q}_\perp\to\infty$.

We are now in a position to derive the parton model for deep-inelastic electron-nucleon scattering. From

(a) (b)

FIG. 9. Examples of electromagnetic vertex corrections which do not contribute in the Bjorken limit. In this work, based on old-fashioned perturbation diagrams, the vertices are all time ordered. A dashed vertical line in a diagram signifies that we are computing the absorptive part describing the production of real multiparticle states. For the left (right) half of such a diagram, the positive time direction is from left (right) to right (left).

here on it will be understood that in (49) we retain only contributions (or diagrams) which do not vanish in the infinite-momentum frame and in the Bjorken limit. We also work with the good components of the current j_μ with $\mu=0$ or 3. Under the fundamental assumption that the particles emitted or absorbed at any strong vertex have only limited transverse momenta, both $|UP\rangle$ and $U|n\rangle$ can be treated as eigenstates of the Hamiltonian with eigenvalues E_p and E_n, respectively. To show this, let E_{um} symbolically denote the energy of one of the multipion-plus-nucleon states in the perturbation expansion of $U|m\rangle$. In the infinite-momentum frame, E_p-E_{up} (as well as E_n-E_{un}) is of the order of $1/P$ multiplied by the sum of squares of some characteristic mass. For example, consider Fig. 7(c). Here $|UP\rangle$ denotes a state of one nucleon and one pion with momenta $\mathbf{P}_1$ and $\mathbf{k}_1$, respectively. The final state $|n\rangle$ contains one nucleon and two pions with momenta $\mathbf{P}_2$, $\mathbf{k}_1$, and $\mathbf{k}_2$, respectively. The state $U|n\rangle$ contains one nucleon and one pion with momenta $\mathbf{P}_1'$ and k_1, respectively. The fractions of the longitudinal momenta carried by these particles are positive and between 0 and 1 as we have shown already. Using (52), we find as $P\to\infty$

$$E_p-E_{up}=\left(P+\frac{M^2}{2P}\right)-\left(\eta_1 P+\frac{k_{1\perp}^2+M^2}{2\eta_1 P}\right)-\left((1-\eta_1)P+\frac{k_{1\perp}^2+\mu^2}{2(1-\eta_1)P}\right)$$
$$=-\frac{1}{2\eta_1(1-\eta_1)P}\times[k_{1\perp}^2+M^2(1-\eta_1)^2+\mu^2\eta_1], \quad (55)$$

$$E_n-E_{un}=\left(\eta_2 P_1'+\frac{k_{2\perp}^2+M^2}{2\eta_2 P_1'}\right)+\left((1-\eta_2)P_1'+\frac{k_{2\perp}^2+\mu^2}{2(1-\eta_2)P_1'}\right)-\left(P_1'+\frac{M^2}{2P_1'}\right)$$
$$=\frac{1}{2\eta_1\eta_2(1-\eta_2)P}\times[k_{2\perp}^2+M^2(1-\eta_2)^2+\mu^2\eta_2]. \quad (56)$$

The differences in (55) and (56) will generally be negligible[13] in comparison with the photon energy q^0 as given in (48) and therefore can be neglected in the energy delta function $\delta(q^0+E_p-E_n)$ appearing in (49) provided we work in the Bjorken limit, $2M\nu$, $Q^2\gg M^2$ and $k_{\perp\,\max}^2\ll Q^2$.

Having shown that both $|UP\rangle$ and $U|n\rangle$ can be treated as eigenstates of the total Hamiltonian with eigenvalues E_p and E_n, respectively, in the Bjorken limit, the over-all energy-conserving delta function in (49) can be replaced by the energy-conserving delta function across the electromagnetic vertex. One can then make use of the translation operators, completeness of states n, and the unitarity of the U matrix to obtain the parton-model result. We illustrate these steps in the following operations on (49):

$$\lim_{P\to\infty;\,Q^2,\,M\nu\to\infty;\,w\text{ fixed}} W_{\mu\nu}=4\pi^2\frac{E_p}{M}\int(dx)e^{iq\cdot x}\times\sum_n\langle UP|e^{iP\cdot x}j_\mu(0)e^{-iP_n\cdot x}U|n\rangle\times\langle n|U^{-1}j_\nu(0)|UP\rangle$$
$$=4\pi^2\frac{E_p}{M}\int(dx)e^{iq\cdot x}\sum_n\langle UP|j_\mu(x)U|n\rangle\times\langle n|U^{-1}j_\nu(0)|UP\rangle$$
$$=4\pi^2\frac{E_p}{M}\int(dx)e^{+iq\cdot x}\times\langle UP|j_\mu(x)UU^{-1}j_\nu(0)|UP\rangle$$
$$=4\pi^2\frac{E_p}{M}\int(dx)e^{+iq\cdot x}\times\langle UP|j_\mu(x)j_\nu(0)|UP\rangle. \quad (57)$$

It is useful to understand the physics behind this derivation. As schematically indicated in Fig. 8, any final state $|n\rangle$ contains two well-separated and identified groups of particles moving along directions differing in transverse momentum by $\mathbf{q}_\perp$. The invariant mass of each of the two groups is small since the transverse momenta of the constituents do not spread far away from each other. The energy differences between states $|P\rangle$ and $|UP\rangle$, and between states $|n\rangle$ and $U|n\rangle$, are

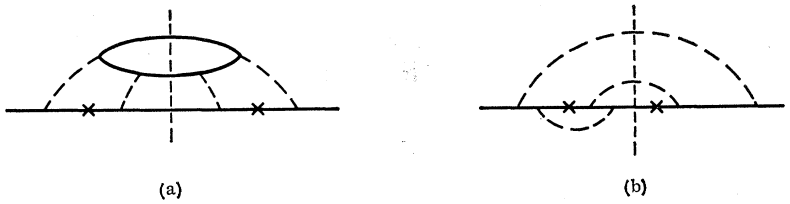

FIG. 10. Examples of diagrams involving interactions between particles in group (A) and those in group (B). These contributions vanish in the Bjorken limit.

therefore negligible in the limit of large Q^2 and $M\nu$. Furthermore, as $Q^2\to\infty$ there is no interaction nor interference between the two groups of particles. The U matrix acts separately and independently on each of the two groups (A) and (B) in Fig. 8. Our derived result (57) simply states the fact that the total probability that anything happens among the particles in each of two groups (A) and (B) is unity because of unitarity of the U matrix. Formally one arrives at the last of equations (57) from the first of (47) by replacing $U^{-1}(t)U(0)\to 1$. In words, this is equivalent to remarking that in the Bjorken limit the interaction occurs during such a short pulse of duration $\approx 1/q_0$ that the strong interactions do not have an opportunity to operate. The electromagnetic current thus "sees" the "bare" constituents or "partons" of the proton in this impulse-approximation limit.

Next we will check to see that the unitarity of the U matrix is preserved in the presence of the finite cutoff that has been introduced into our formalism. To do this, we shall demonstrate by explicit calculations through fourth order in g that when all contributions are summed up, the total probability that anything happens among the individual groups of particles (A) and (B) in Fig. 8 is unity because of unitarity of U. This verifies that $U|n\rangle\to|n\rangle$ in (49), and thus that (57) is valid and U is unitary to this order. Three specific examples are offered to support this claim. First, consider the contribution of Fig. 7(c) to $W_{\mu\nu}$. Let this contribution be denoted by $W_{\mu\nu}^{(2)}$. Using (49) and (5), we obtain

$$W_{\mu\nu}^{(2)}=\left(\frac{g^2}{(2\pi)^3}\right)^2\frac{1}{4M}\int\frac{d^3k_1}{2\omega_1}\frac{d^3k_2}{2\omega_2}\frac{1}{2E_1'}\delta(q^0+E_p-E_2-\omega_1-\omega_2)$$
$$\times\frac{\mathrm{Tr}\{(M+\gamma P)\gamma_5(M+\gamma P_1)\gamma_\mu(M+\gamma P_1')\gamma_5(M+\gamma P_2)\gamma_5(M+\gamma P_1')\gamma_\nu(M+\gamma P_1)\gamma_5\}}{(2E_1)^2(E_p-E_1-\omega_1)^2(2E_1')(2E_2)(E_2+\omega_2-E_1')^2},\quad(58)$$

where the pions are assumed to be all neutral and the momentum labels are those indicated in Fig. 7(c). Using (48) and (42), we have in the Bjorken limit

$$(1/2E_1')\delta(q^0+E_p-E_2-\omega_1-\omega_2)=\delta(2M\nu\eta_1-Q^2)=\delta(2P_1\cdot q+q^2).\quad(59)$$

Furthermore,

$$(M+\gamma P_1')\gamma_5(M+\gamma P_2)\gamma_5(M+\gamma P_1')=(+2)(M^2-P_1'\cdot P_2)(M+\gamma P_1').\quad(60)$$

Hence

$$W_{\mu\nu}^{(2)}=(1-Z_{2(\pi^0)})\left(\frac{g^2}{(2\pi)^3}\right)\frac{-1}{4M}\int\frac{d^3k_1}{2\omega_1}\delta(q^2+2P_1\cdot q)\frac{\mathrm{Tr}\{(M+\gamma P)\gamma_5(M+\gamma P_1)\gamma_\mu[M+\gamma(P_1+q)]\gamma_\nu(M+\gamma P_1)\gamma_5\}}{(2E_1)^2(E_p-E_1-\omega_1)^2},\quad(61)$$

where $Z_{2(\pi^0)}$ is given by (18) provided we identify the cutoffs introduced in (61) and (18). Equation (61) can be rewritten as

$$W_{\mu\nu}^{(2)}+Z_{2(\pi^0)}W_{\mu\nu}^{(1)}=W_{\mu\nu}^{(1)},\quad(62)$$

where $W_{\mu\nu}^{(1)}$ is easily verified to be the contribution of Fig. 12(a) to $E_{\mu\nu}$. When the charged pion is included, (62) becomes

$$W_{\mu\nu}^{(2)}+Z_2W_{\mu\nu}^{(1)}=W_{\mu\nu}^{(1)},\quad(63)$$

where $W_{\mu\nu}^{(2)}$ now stands for the *total* contribution to $W_{\mu\nu}$ when the pion with momentum k_2 in Fig. 7(c) is neutral as well as charged; and Z_2 is the product of $Z_{2(\pi^0)}$ and $Z_{2(\pi^+)}$; i.e., $Z_2=Z_{2(\pi^0)}+Z_{2(\pi^+)}-1\approx Z_{2(\pi^0)}Z_{2(\pi^+)}$ to order g^2.

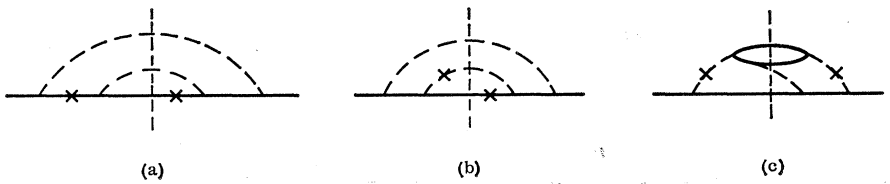

FIG. 11. Examples of diagrams involving interferences between two different configurations of final particles (A), (B) and (A'), (B').

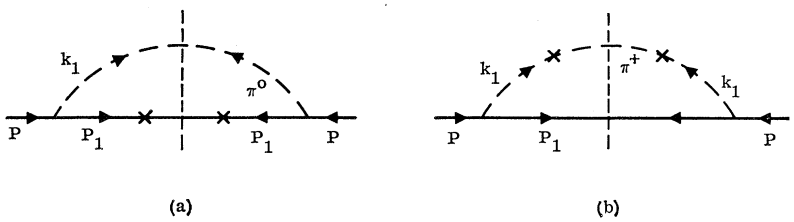

FIG. 12. Second-order contributions to $W_{\mu\nu}$ from the nucleon current (a) and the pion current (b).

The contribution of Fig. 7(d) to $W_{\mu\nu}$ can also be calculated similarly. Let $W_{\mu\nu}^{(2')}$ denote this contribution. It is given by

$$W_{\mu\nu}^{(2')}=\left(\frac{g^2}{(2\pi)^3}\right)^2\frac{1}{2M}\int\frac{d^3k_1}{2\omega_1}\frac{d^3p_2}{2E_2}\delta(q^2+2P\cdot_1 q)\frac{\mathrm{Tr}\{(M+\gamma P)\gamma_5(M+\gamma P_1)\gamma_\mu[M+\gamma(P_1+q)]\gamma_\nu(M+\gamma P_1)\gamma_5\}}{(2E_1)^2(E_p-E_1-\omega_1)^2}$$
$$\times\frac{\mathrm{Tr}\{(M+\gamma P_2)\gamma_5(-M+\gamma\bar{P}_2)\gamma_5\}}{(2\omega_1)(2\bar{E}_2)(\omega_1-E_1-\bar{E}_2)^2},\quad(64)$$

where both the $P\bar{P}$ and $N\bar{N}$ intermediate states are included in (64). This can be rewritten as

$$W_{\mu\nu}^{(2')}+Z_3W_{\mu\nu}^{(1)}=W_{\mu\nu}^{(1)},\quad(65)$$

where $W_{\mu\nu}^{(1)}$ is again the contribution of Fig. 12 to $W_{\mu\nu}$, and Z_3 is given by (20). To order g^2, the wave-function renormalization constant Z' of a one-nucleon plus one-pion state defined by

$$U|P_1k_1\rangle=(\sqrt{Z'})\{|P_1k_1\rangle+\cdots\}\quad(66)$$

is related to Z_2 and Z_3 by

$$Z'=Z_2Z_3\simeq Z_2+Z_3-1.\quad(67)$$

Adding (63) and (65), we obtain

$$W_{\mu\nu}^{(2)}+W_{\mu\nu}^{(2')}+Z'W_{\mu\nu}^{(1)}=W_{\mu\nu}^{(1)}.\quad(68)$$

Equation (68) is an example displaying that after summation over all possible final states, the U matrices adjacent to the final states in (49) may be replaced by unity; i.e., $U|n\rangle\rightarrow|n\rangle$. The graph drawn in Fig. 13(a) was not included in this discussion since the perturbation series (5) leads only to intermediate states differing from the one on which U operates, which in this case is the state $|n\rangle$ of one nucleon plus pion as illustrated. In contrast, the two graphs in Figs. 14(b) and 13(c) do occur and combine to renormalize the strong coupling constant g in the usual fashion. Also, because of our finite cutoff for transverse momenta, the amplitude corresponding to Fig. 9(a) vanishes as $Q^2\rightarrow\infty$. Although the bare charge e_0 appears at the electromagnetic vertex, to lowest order, however, in the electromagnetic interaction e_0 is identical with the physical charge e. In accord with the Ward identity, $Z_1=Z_2$ as verified to lowest order in Sec. II, and the photon's vacuum polarization enters only to higher order in the fine-structure constant. Therefore, as long as we have current conservation in our general formalism, as insured by constructing the form (47), $e_0=e$ is the physical charge at the electromagnetic vertex. In this example, we considered the nucleon-current contributions. A similar discussion applies to the pion-current contributions of Figs. 7(g), 7(h), and 12(b). The result is analogous to (68).

For the third example, we consider the contributions of Figs. 14(a) and 14(b) to $W_{\mu\nu}$. Let these contributions be $W_{\mu\nu}^{(a)}$ and $W_{\mu\nu}^{(b)}$, respectively; then

$$W_{\mu\nu}^{(a)}=\frac{g^2}{(2\pi)^3}\frac{1}{2M}\int\frac{d^3k_2}{2\omega_2}\frac{d^3p_2}{2E_2}\frac{1}{2\omega_{k_1+q}}\delta(q^0+\omega_1-\omega_{k_1}+q)(2k_1+q)_\mu(2k_1+q)_\nu$$
$$\times\frac{\mathrm{Tr}\{(M+\gamma P)\gamma_5(M+\gamma P_1)\gamma_5(M+\gamma P_2)\gamma_5(M+\gamma P_1)\gamma_5\}}{(2E_1)^2(E_p-E_1-\omega_1)^2(2\omega_1)^2(E_2+\omega_2-E_1)(E_p-E_2-\omega_1-\omega_2)},\quad(69)$$

$$W_{\mu\nu}^{(b)}=\frac{g^2}{(2\pi)^3}\frac{1}{2M}\int\frac{d^3k_2}{2\omega_2}\frac{d^3p_2}{2E_2}\frac{1}{2\omega_{k_1+q}}\delta(q^0+\omega_1-\omega_{k_1}+q)(2k_1+q)_\mu(2k_1+q)_\nu$$
$$\times\frac{\mathrm{Tr}\{(M+\gamma P)\gamma_5(M+\gamma P_1)\gamma_5(M+\gamma P_2)\gamma_5(M+\gamma P_1)\gamma_5\}}{(2E_1)^2(E_p-E_1-\omega_1)^2(E_1-E_2-\omega_2)(E_p-E_2-\omega_1-\omega_2)},\quad(70)$$

where $\omega_{k_1+q}=[(\mathbf{k}_1+\mathbf{q})^2+\mu^2]^{1/2}$; and we have replaced the over-all energy-conserving delta function by the energy-conserving delta function across the electromagnetic vertex in the Bjorken limit. The only differ-

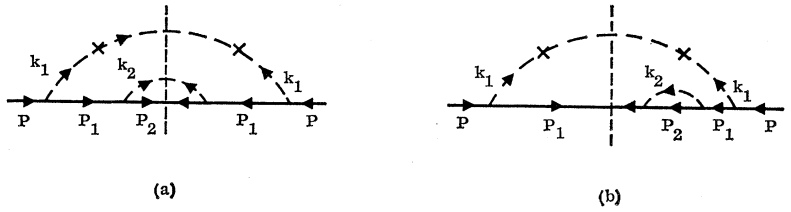

FIG. 13. An example of graphs in a fourth-order calculation that add to zero, indicating that the total effect of U operating on states $|n\rangle$ *after* the interaction with the electromagnetic current, represented by the ✕, can be replaced by unity—i.e., $U|n\rangle \to |n\rangle$.

ence between (69) and (70) is that one of the energy denominator changes sign. Thus

$$W_{\mu\nu}{}^{(a)}+W_{\mu\nu}{}^{(b)}=0, \tag{71}$$

which verifies again our assertion that unitarity of the U matrix permits us to ignore the U matrices acting on the final states $|n\rangle$ in (49).

From these examples we see that to preserve the unitarity of the U matrix, it is crucial to identify the transverse momentum cutoff for the real final particles appearing in (49) with the transverse momentum cutoff for the virtual particles in the internal loops of renormalization integrals. Experimental data on high-energy collisions indicate that the transverse momenta of the final real particles are limited in magnitude. By the self-consistent requirement of preserving the unitarity of the U matrix, it follows that the virtual particles must also have only limited transverse momenta.

The result of Eq. (57) establishes the parton model by allowing us to work with free point currents and the superposition of essentially free (i.e., long-lived) constituents in describing the proton's ground state in the infinite-momentum frame and in the Bjorken limit. It also leads to a universal behavior of W_1 and νW_2 as functions of w, as predicted by Bjorken[3] and discussed on the basis of this model in Refs. 1 and 2. To exhibit explicitly that in the Bjorken limit both W_1 and νW_2 become functions of w only, we expand $|UP\rangle$ in terms of a complete set of multiparticle states

$$|UP\rangle=\textstyle\sum_n a_n|n\rangle, \quad \sum_n |a_n|^2=1. \tag{72}$$

As we have shown in the preceding discussion, the evaluation of (57) involves only *diagonal* elements of the product of the bare currents in the Bjorken limit ($\lim_{Bj}$), i.e.,

$$\lim_{Bj} W_{\mu\nu}=4\pi^2\frac{E_p}{M}\textstyle\sum_n |a_n|^2\int (dx)e^{iq\cdot x} \times\langle n|j_\mu(x)j_\nu(0)|n\rangle. \tag{73}$$

Since j_μ is a one-body operator, the evaluation of (73) boils down to a calculation of a sum of contributions from each charged constituent in every state $|n\rangle$. Thus, for a nucleon-current term,

$$\int (dx)e^{+iq\cdot x}\langle P_n,s|j_\mu(x)j_\nu(0)|P_n,s'\rangle=\frac{1}{4\pi^2}\frac{M}{E_n}\bar{u}_{pn}(s)\gamma_\mu \times[M+\gamma(P_n+q)]\gamma_\nu u_{pn}(s')\delta(q^2+2P_n\cdot q), \tag{74}$$

where $|P_n,s\rangle$ is a one-proton state with momentum P_n and spin s; and for a pion-current contribution,

$$\int (dx)e^{+iq\cdot x}\langle k_n|j_\mu(x)j_\nu(0)|k_n\rangle =\frac{1}{4\pi^2}\frac{1}{2\omega_n}(2k_{n\mu}+q_\mu)(2k_{n\nu}+q_\nu)\delta(q^2+2k_n\cdot q), \tag{75}$$

where $|k_n\rangle$ is a one-charged-pion state with momentum k_n. The symmetry of $W_{\mu\nu}$ in indices $\mu\nu$ allows us to extract the tensor structure in (74) easily. Commuting γ_μ or γ_ν through $[M+\gamma(P_n+q)]$, replacing $\gamma_\mu\gamma_\nu$ by its symmetrical part $g_{\mu\nu}$, making use of Dirac equation, and neglecting terms proportional to q_μ or q_ν (which make no contribution to the cross section after contraction with the lepton trace), we obtain[14]

$$\int (dx)e^{+iq\cdot x}\langle P_n,s|j_\mu(x)j_\nu(0)|P_n,s'\rangle =\delta_{ss'}\frac{1}{4\pi^2}\frac{1}{2E_n}[-g_{\mu\nu}Q^2+4P_{n\mu}P_{n\nu}]\delta(q^2+2P_n\cdot q). \tag{76}$$

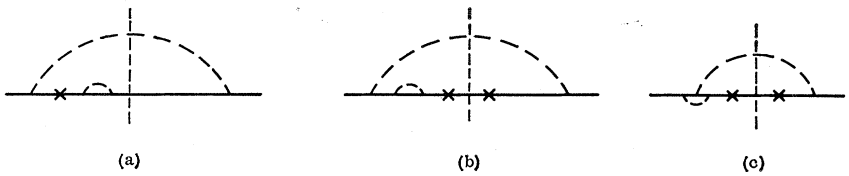

FIG. 14. Examples of diagrams to illustrate the difference between old-fashioned perturbation and covariant perturbation calculations. In the old-fashioned theory (a) is explicitly excluded but its effect is properly taken into account by the wave-function renormalization constant Z_a in (5). (b) and (c) combine to renormalize the strong-coupling constant g in the usual fashion.

[14] Equation (76) still holds if the proton is replaced by an antiproton.

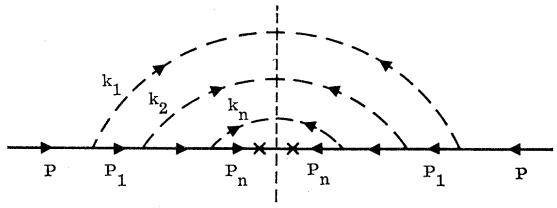

FIG. 15. Dominant ladder diagrams for large w.

The δ functions in (75) and (76) express the fact that when the bare current j_μ lands on a "parton" or almost free charged constituent with momentum p_a, $p_a{}^2=m_a{}^2$, it scatters it onto the mass shell with p_a+q and $(p_a+q)^2=m_a{}^2$. It can be further simplified by writing, to leading order in $P\to\infty$, $\mathbf{p}_a=\eta_a\mathbf{P}$, where η_a is the fraction of longitudinal momentum borne by the constituent on which the current lands; then we have

$$\delta(2p_a\cdot q-Q^2)=\delta(2\eta_a M\nu-Q^2)$$
$$=(1/2M\nu)\delta(\eta_a-1/w). \quad (77)$$

Independent of details of the strong-interaction dynamics, the parton which interacts with the current must have the fraction $1/w$ of the longitudinal momentum according to (77). Collecting together (75)–(77) into (73), and denoting by $\lambda_i{}^F$ the charge of the ith fermion (nucleon or antinucleon in our model) and by $\lambda_j{}^B$ the charge of the jth spinless boson (pion in our model), we arrive at

$$W_{\mu\nu}=\frac{1}{w}\sum_n|a_n|^2\langle n|\left\{\frac{P_\mu P_\nu}{\nu M^2}\sum_j(\lambda_j{}^B)^2\delta\left(\eta_j-\frac{1}{w}\right)\right.$$
$$\left.+\left(\frac{P_\mu P_\nu}{\nu M^2}-g_{\mu\nu}\frac{w}{2M}\right)\sum_i(\lambda_i{}^F)^2\delta\left(\eta_i-\frac{1}{w}\right)\right\}|n\rangle. \quad (78)$$

Referring to the scalar structure functions as defined in (47), we see that W_1 and νW_2 are, as claimed, functions only of w. Furthermore, their observed w dependence "measures" the longitudinal momentum distribution of the charged constituents of the proton in the infinite-momentum frame. The ratio of W_1 to νW_2 in (78) has a fixed value for the nucleon current:

$$W_1/\nu W_2=w/2M \quad \text{(nucleon current)}. \quad (79a)$$

The pion current contributes only to W_2, and

$$W_1=0 \quad \text{(pion current)}. \quad (79b)$$

The dynamical details of the theory determine the relative contributions from the nucleon and pion currents and hence the ratio of W_1 to νW_2 in the observed cross sections.

With the derivation of (78) and (79) establishing that in the Bjorken limit the structure functions are universal functions of w, we have completed the first major task of this paper. Sometimes we shall find it convenient to employ the notation in I:

$$F_1(w)=\lim_{\mathrm{Bj}} MW_1(q^2,\nu),$$
$$F_2(w)=\lim_{\mathrm{Bj}} \nu W_2(q^2,\nu). \quad (80)$$

Equation (78) gives a sum rule

$$\int_1^\infty\frac{dw}{w}F_2(w)=\sum_n\left(\sum_i\lambda_{n,i}{}^2\right)|a_n|^2$$
$$=\sum_n n_c|a_n|^2$$
$$\equiv\langle n_c\rangle, \quad (81)$$

where n_c is the number of charged constituents bosons plus fermions in state $|n\rangle$. We have here implicitly assumed that the constituents are either neutral or have unit charge as is the case in our model. Thus, the weighted integral of $F_2(w)$, (81), may be interpreted as the mean number of charged constituents in the physical nucleon. For a proton, $n_c\geq 1$ and thus the normalization condition (72) on the a_n's leads to the inequality

$$\int_1^\infty\frac{dw}{w}F_2(w)\geq 1. \quad (82)$$

This inequality is trivial to satisfy if the SLAC data[5] continue their present trend, since νW_2 or $F_2(w)$ varies very slowly for large w and even may be approaching a constant. Thus far, with measurements extending to $w_{\max}\sim 20$, the area under the integral is roughly ~ 0.7 from $1\leq w\leq w_{\max}$. Equation (82) shows that the result presented by (57) is actually finite and nonvanishing—i.e., the Bjorken limit is a nontrivial result.

We may also remark briefly concerning the possible existence of spin-1 constituents. There is no difficulty to incorporate *neutral* spin-1 constituents in our formalism provided a transverse momentum cutoff is also introduced for vertices involving these spin-1 constituents. This will be done in Sec. IV. Difficulty will arise, however, if *charged* spin-1 constituents are present due to the extra q dependence at the electromagnetic vertex introduced by the higher spin and the derivative electromagnetic coupling. This has the consequence that the Bjorken limit for $W_{\mu\nu}$ will not exist for contributions from the electromagnetic current of spin-1 charged constituents. One may accept the experimental data from SLAC as an indication that a Bjorken limit indeed exists for $W_{\mu\nu}$, to conclude that spin-1 charged constituents of the proton, if any, contribute negligibly to deep-inelastic electron-proton scattering. Similarly, specific Pauli anomalous moment interactions of the elementary spin-$\frac{1}{2}$ constituents are ruled out.

IV. ASYMPTOTIC BEHAVIOR OF STRUCTURE FUNCTIONS FOR LARGE w

In Ref. 1 we claimed that in the Bjorken limit and in the large-w region the structure functions $F_{1,2}(w)$ are,

order by order in g^2, dominated by a simple class of diagrams, namely, the ladder diagrams with pion lines as the rungs and with the nucleon interacting with the current. In this section, we shall first sum up these leading contributions to each order in g^2 from the ladder diagrams to all orders and then supply the arguments which support our claim. The charged pions will be completely ignored first, since they can be taken into account later by a simple consideration, and consider the proton. The contribution from a diagram as in Fig. 15, involving n π^0's in the final state, is obtained by introducing

$$U_{(n\pi^0)}(0)|P\rangle=\left(\frac{g}{(2\pi)^{3/2}}\right)^n(n!)^{1/2}\frac{2M}{(2E_p)^{1/2}}\int\frac{d^3P_n}{(2E_n)^{1/2}}\prod_{i=1}^n\frac{d^3k_i}{(2\omega_i)^{1/2}}\delta^3(\mathbf{P}-\mathbf{P}_n-\mathbf{k}_1-k_2\cdots\mathbf{k}_n)|P_nk_1\cdots\mathbf{k}_n\rangle$$
$$\times\frac{\bar{u}_{pn}\gamma_5(M+\gamma P_{n-1})\gamma_5\cdots\gamma_5(M+\gamma P_1)\gamma_5u_p}{(2E_1)\cdots(2E_{n-1})(E_p-E_1-\omega_1)\cdots(E_p-E_n-\omega_1\cdots-\omega_n)} \tag{83}$$

into (57) and using (75). Only $F_2(w)$ or νW_2 needs to be considered, since $F_1(w)$ or W_1 is given by (79a). Thus we have

$$F_2(w)_{(n\pi^0)}=\left(\frac{g^2}{(2\pi)^3}\right)^nM\nu\int\prod_{i=1}^n\frac{d^3k_i}{2\omega_i}\delta(q^2+2P_n\cdot q)\left(\frac{E_n}{E_p}\right)^2$$
$$\times\frac{\mathrm{Tr}\{(M+\gamma P)\gamma_5(M+\gamma P_1)(M+\gamma P_{n-1})\gamma_5(M+\gamma P_n)\gamma_5(M+\gamma P_{n-1})\cdots\gamma_5(M+\gamma P_1)\gamma_5\}}{(2E_1)^2\cdots(2E_n)^2(E_p-E_1-\omega_1)^2\cdots(E_p-E_n-\omega_1\cdots-\omega_n)^2}. \tag{84}$$

The trace may be evaluated with the aid of the following identity for two on-shell momenta P_1 and P_2:

$$(M-\gamma P_1)(M+\gamma P_2)+(M+\gamma P_2)(M-\gamma P_1)=2(M^2-P_1P_2). \tag{85}$$

The result is

$$\mathrm{Tr}\{(M+\gamma P)\gamma_5(M+\gamma P_1)\cdots\gamma_5(M+\gamma P_{n-1})\gamma_5(M+\gamma P_n)\gamma_5(M+\gamma P_{n-1})\gamma_5\cdots(M+\gamma P_1)\gamma_5\}$$
$$=2(-2)^n(M^2-P\cdot P_1)(M^2-P_1\cdot P_2)\cdots(M^2-P_{n-1}\cdot P_n). \tag{86}$$

Let us parametrize the momenta as follows:

$$\mathbf{P}_i=\eta_i\mathbf{P}_{i-1}+\mathbf{k}_{i\perp},\quad \mathbf{k}_i=(1-\eta_i)\mathbf{P}_{i-1}-\mathbf{k}_{i\perp},\quad \mathbf{k}_{i\perp}\cdot\mathbf{P}_{i-1}=0,$$
$$0<\eta_i<1,\quad i=1,2,\cdots,n\quad (P_{i-1}\equiv P \text{ for } i=1). \tag{87}$$

Then

$$(-2)(M^2-P_{i-1}\cdot P_i)=\frac{1}{\eta_i}[(k_{i\perp}-\eta_ik_{i-1})^2+M^2(1-\eta_i)^2],$$
$$E_{i-1}-E_i-\omega_i=\frac{-1}{2\eta_1\cdots\eta_i(1-\eta_i)P}[k_{i\perp}^2+M^2(1-\eta_i)^2+\mu^2\eta_i]. \tag{88}$$

Equations (84), (86), and (88) give

$$F_2(w)_{(n\pi^0)}=\left(\frac{g^2}{2(2\pi)^3}\right)^n\int\prod_{i=1}^n d^2k_{i\perp}\int_0^1\prod_{i=1}^n d\eta_i\delta\left(\eta_1\cdots\eta_n-\frac{1}{w}\right)\eta_1\cdots\eta_n$$
$$\times\left\{\frac{(1-\eta_1)\cdots(1-\eta_n)[k_{1\perp}^2+M^2(1-\eta_1)^2]\cdots[k_{n\perp}^2+M^2(1-\eta_n)^2]}{[k_{1\perp}^2+M^2(1-\eta_1)^2+\mu^2\eta_1]^2\{[\eta_2(1-\eta_2)/(1-\eta_1)][k_{1\perp}^2+M^2(1-\eta_1)^2+\mu^2\eta_1]+[k_{2\perp}^2+M^2(1-\eta_2)^2+\mu^2\eta_2]\}^2}\right.$$
$$\left.\times\cdots\frac{1}{\{[\eta_2\cdots\eta_n(1-\eta_n)/(1-\eta_1)][k_{1\perp}^2+M^2(1-\eta_1)^2+\mu^2\eta_1]+\cdots+[k_{n\perp}^2+M^2(1-\eta_n)^2+\mu^2\eta_n)]\}^2}\right\}. \tag{89}$$

Hence

$$F_2(w)_{(n\pi^0)}=\left(\frac{g^2}{2(2\pi)^3}\right)^n\frac{1}{w}\int\prod_{i=1}^n d^2k_{i\perp}\int_{1/w}^1\frac{d\eta_1}{\eta_1}\int_{1/\eta_1w}^1\frac{d\eta_2}{\eta_2}\cdots\int_{1/\eta_1\cdots\eta_{n-2}w}^1\frac{d\eta_{n-1}}{\eta_{n-1}}\{\cdots\}, \tag{90}$$

where $\{\cdots\}$ denotes the expression in the large curly brackets of (89), with $\eta_n=1/\eta_1\cdots\eta_{n-1}w$. Introduce the new variables

$$\begin{aligned}\eta_1&=(1/w)^{\eta_1'}, &&0<\eta_1'<1\\ \eta_1\eta_2&=(1/w)^{\eta_2'}, &&\eta_1'<\eta_2'<1\\ &\cdots &&\cdots\\ \eta_1\cdots\eta_{n-1}&=(1/w)^{\eta_{n-1}'}, &&\eta_{n-2}'<\eta_{n-1}'<1\end{aligned}$$

and notice

$$\int_{1/w}^1\frac{d\eta_1}{\eta_1}\int_{1/\eta_1\cdots\eta_{n-1}w}^1\frac{d\eta_{n-1}}{d_{n-1}}\{\cdots\}=(\ln w)^{n-1}\times\int_0^1 d\eta_1'\int_{\eta_1'}^1 d\eta_2'\cdots\int_{\eta_{n-2}'}^1 d\eta_{n-1}'\{\cdots\}. \quad (91)$$

Here we have succeeded in exhibiting the dominant dependence of $F_2(w)$ on w as $w\to\infty$. The limit $w\to\infty$ can now be taken in the integrand. Since

$$\eta_1=(1/w)^{\eta_1'}\to 0 \quad \text{as} \quad w\to\infty \quad \text{for} \quad 0<\eta_1'<1,$$
$$\eta_2=(1/w)^{\eta_1'-\eta_2'}\to 0 \quad \text{as} \quad w\to\infty \quad \text{for} \quad \eta_1'<\eta_2'<1,$$
$$\text{etc.},$$

we set all the η's in the integrand $\{\cdots\}$ to zero and obtain

$$F_2(w)_{(n\pi^0)}\xrightarrow[w\to\infty]{}\left(\frac{g^2}{16\pi^2}\right)^n\left(\int\frac{dk_\perp^2}{k_\perp^2+M^2}\right)^{n-1}\frac{1}{w}(\ln w)^{n-1}\times\int_0^1 d\eta'\cdots\int_{\eta_{n-2}'}^1 d\eta_{n-1}'=\frac{\xi_0}{w}\frac{1}{(n-1)!}(\xi_0\ln w)^{n-1}, \quad (92)$$

$$F_1(w)_{(n\pi^0)}=\tfrac{1}{2}wF_2(w)_{(n\pi^0)}, \quad (93)$$

where

$$\xi_0\equiv\frac{1}{4\pi}\left(\frac{g^2}{4\pi}\right)\ln\left(1+\frac{(k_\perp^2)_{\max}}{M^2}\right), \quad (94)$$

and $k_{\perp\,\max}$ is a cutoff introduced for the transverse momentum integrals in accordance with our fundamental assumption. Summing over all numbers of π^0's, we find

$$F_2(w)_{(\pi^0)}=(\xi_0/w)\exp(\xi_0\ln w)=\xi_0 w^{\xi_0-1}. \quad (95)$$

To include the charged pions in the calculation, we observe that an initial proton can emit a π^0 and remain as a proton with coupling constant g or it can emit a π^+ and become a neutron with a coupling constant $\sqrt{2}g$. An analogous situation applies to a neutron. Let the contribution from a final state with n π^0's and a proton be taken as the basic unit, and denote the total numbers of contributions from all possible final states with n charged-plus-neutral pions by P_n and N_n for the proton and neutron, respectively. They satisfy the recursion relations

$$P_n=P_{n-1}+2N_{n-1}, \quad N_n=2P_{n-1}+N_{n-1}. \quad (96)$$

These give

$$\begin{aligned}P_n+N_n&=3^{n-1}(P_1+N_1),\\ P_n-N_n&=(-1)^{n-1}(P_1-N_1).\end{aligned} \quad (97)$$

By explicit counting,

$$P_1=1, \quad N_1=2. \quad (98)$$

Finally,

$$P_n+N_n=3^n, \quad P_n-N_n=(-1)^n, \quad (99)$$

which convert (95) to

$$F_2(w)^{(p)}=F_2(w)^{(n)}=\tfrac{1}{2}c\xi w^{\xi-1}, \quad (100)$$

$$F_2(w)^{(p)}-F_2(w)^{(n)}=-\tfrac{1}{3}c\xi w^{-(\xi/3+1)}, \quad (101)$$

and

$$F_1(w)=\tfrac{1}{2}wF_2(w), \quad (102)$$

where

$$\xi=\frac{3}{4\pi}\left(\frac{g^2}{4\pi}\right)\ln\left(1+\frac{(k_\perp^2)_{\max}}{M^2}\right) \quad (103)$$

and the constant c is not fixed by summing a leading exponential series of powers of $\ln w$.

Contributions of all other diagrams in the $P\to\infty$ system are smaller by at least one power of $\ln w$, order by order in g^2. This follows from the parton-model result (57) and the properties of the pion-nucleon vertex with a transverse momentum cutoff in an infinite-momentum frame, (9). Explicit verification of our assertion has been carried out to g^4 for all diagrams. The complete g^4 calculation is straightforward and tedious. We shall assemble explicit results in the Appendix for reference since they will be needed when we study the crossing properties of the structure functions W_1 and W_2 in our next paper on electron-positron annihilation processes.

To understand in general why the contributions of diagrams other than the ladder ones with interactions via the nucleon current are smaller at least by one power of $\ln w$ as $w\to\infty$, we recall from (9) that at each nucleon vertex with γ_5 coupling to pseudoscalar pions, the nucleon likes to give up most of its momentum to the pion. In fact, according to (9), the $(\ln w)^{n-1}$ behavior in (92) comes simply from the fact that each segment of the nucleon line has but a small fraction $\eta\ll 1$ of the longitudinal momentum of the one preceding it in Fig. 15. Moreover, the delta function in (89) tells us that the η's measuring the fraction of energy retained by the nucleons are small for $w\gg 1$. However, when the currents are attached to a pion line, the delta function would dictate that a *pion* and not the nucleon pick up a small fraction $\sim 1/w$ of the longitudinal momentum from the initial nucleon, in the large-w region. This is not favored by the vertex, and hence at least one power of $\ln w$ is lost.

If two pion lines cross each other in a diagram, the two virtual nucleons which connect the two pion lines on each side have a momentum mismatch; i.e., if a nucleon on one side picks up a small fraction of the available longitudinal momentum, the nucleon on the other side has to pick up a large fraction by momentum conservation. For a diagram with a final state involving nucleon-antinucleon pairs, the virtual pion creating the

pair is favored to have a large fraction of the available longitudinal momentum. For a Z diagram (an antinucleon or nucleon moving backward in time), the vertex favors a high-momentum virtual nucleon (or antinucleon). In all these cases at least one virtual particle has a large fraction of the longitudinal momentum available; thus at least one power of $\ln w$ is lost. For a vertex correction diagram such as Fig. 17(a) one has added a power of g^2 without gaining an additional power of $\ln w$ along with it. For example, let most of the longitudinal momentum of the initial nucleon be picked up by the first virtual pion so that the vertex is as big as possible. By the very nature of this being a virtual pion, this large longitudinal momentum must be returned to a nucleon before the nucleon interacts with the current. Yet as $1/w \to 0$ this nucleon can have only a very small fraction of longitudinal momentum from the initial proton; in fact, this fraction is precisely $1/w$. Thus, it is impossible to make *all* the vertices large. All other diagrams can be understood by this simple type of argument. Having exhausted all possible classes of diagrams, we now have *derived* the ladder approximation for the leading term order by order when $w \gg 1$.

This structure for the asymptotically leading contributions, order by order in g^2, is independent of the specific property of the coupling (γ_5) and spin of the pion (zero) used in this example. By explicit calculation it is easy to show this property for scalar mesons with scalar coupling and, in a manner similar to the above, derive the same structure as (95) for scalar spinless bosons. Indeed, for any coupling via the so-called "bad currents," the nucleon prefers in the relativistic limit to transfer the maximum possible fraction of its longitudinal momentum to the boson.

To demonstrate that the formal structure of the result (95) for $w \gg 1$ is not sensitive to the spin of the constituents and also to simulate possible final-state-interaction effects of the pions, we consider briefly a model in which the proton interacts strongly with *neutral* vector mesons which we call ρ^0. The interaction Hamiltonian is taken as

$$H_I = g' \int d^3x\, \bar{\psi}_p \gamma_\mu \psi_p \phi^\mu + \frac{g'^2}{2\mu^2} \int d^3x\, (\bar{\psi}_p \gamma_0 \psi_p)^2 ,$$

where ϕ^μ is the vector field for the spin-1 particle; the second term appears because the interaction Lagrangian (given by the first term in this case) generally differs from the interaction Hamiltonian for couplings with particles of spin ≥ 1. Similar analysis shows that as $w \to \infty$ the ladder diagrams of Fig. 13 also dominate in this case. The contribution from a diagram involving n ρ^0's in the final state is

$$F_2(w)_{(n\rho^0)} = \left(\frac{g'^2}{2(2\pi)^3}\right)^n M\nu \int \prod_{i=1}^{n} \frac{d^3k_i}{2\omega_i} \delta(q^2 + 2P_n \cdot q) \left(\frac{E_n}{E_p}\right)^2 \times \sum_{\epsilon_1 \cdots \epsilon_2} \frac{\mathrm{Tr}\{(M+\gamma P)\gamma\epsilon_1 (M+\gamma P_1) \cdots \gamma\epsilon_n (M+\gamma P_n)\gamma\epsilon_n \cdots (M+\gamma P_1)\gamma\epsilon_1\}}{(2E_1)^2 \cdots (2E_n)^2 (E_p - E_1 - \omega_1)^2 \cdots (E_p - E_n - \omega_1 - \cdots \omega_n)^2} , \quad (104)$$

where the momentum labels are the same as in Fig. 15 with pions replaced by vector mesons; and $\epsilon_1 \cdots \epsilon_n$ are the polarization vectors for the n vector mesons. The polarization sum and the trace can be evaluated to obtain

$$\sum_{\epsilon_1 \cdots \epsilon_n} \mathrm{Tr}\{(M+\gamma P)\gamma\epsilon_1 \cdots \gamma\epsilon_n (M+\gamma P_n)\gamma\epsilon_n \cdots (M+\gamma P_1)\gamma\epsilon_1\} = 2[-2(M^2 - P \cdot P_1) + 4\mu^{-2}(P \cdot k_1)(P_1 \cdot k_1) - 4M^2]$$
$$\times [-2(M^2 - P_1 \cdot P_2) + 4\mu^{-2}(P_1 \cdot k_2)(P_2 \cdot k_2) - 4M^2] \cdots [-2(M^2 - P_{n-1} \cdot P_n) + 4\mu^{-2}(P_{n-1} \cdot k_n)(P_n \cdot k_n) - 4M^2] . \quad (105)$$

Using the parametrization (87), we obtain as $w \to \infty$

$$F_2(w)_{(n\rho^0)} \xrightarrow[w \to \infty]{} \frac{\xi'}{w} \frac{1}{(n-1)!} [\xi' (\ln w)^{n-1}] . \quad (106)$$

Summing over all numbers of ρ^0, we get

$$F_2(w)_{(\rho^0)} = \xi' w^{\xi' - 1} , \quad (107)$$

where

$$\xi' = \frac{g'^2}{16\pi^2} \int dk_\perp^2 \frac{k_\perp^2 + M^2 + 2\mu^2}{\mu^2 (k_\perp^2 + M^2)} .$$

Equation (107) has exactly the same structure as (95). The point is that the "bad" or transverse components $\gamma = (\gamma_1, \gamma_2)$ of γ_μ dominate in this example and have the same general properties as do the vertices γ_5 and 1 already considered. The nucleon moving along **P** initially will continue with its longitudinal momentum along (rather than antiparallel to) **P** through the interactions as it emits and absorbs bosons, because only then do we retain the maximum possible powers of $\ln w$, one for each order of interaction when the intermediate nucleon line is near the mass shell. At vertices of this kind, $\gamma_\perp$ introduces a factor $(\eta_1/\eta_2)^{1/2}$ when $\eta_2 \ll \eta_1$ in the large-w limit, and the structure of the amplitude is the same as for the spinless case in Eq. (9). The identical conclusion follows for axial-vector mesons with axial-vector coupling $\gamma_\mu \gamma_5$ to nucleons.

We conclude this section with comments on three points.

(a) The results of this section, based as they are on a procedure of summing only the individual leading terms *both* in $Q^2 \gg M^2$ and $\ln w \gg 1$ in an infinite series, are on a less firm basis than is our general procedure for deriving the scaling laws for the structure functions. Being more speculative they are more suspect. They may very well meet the same ignominious fate as the unsuccessful attempts to study asymptotic behaviors of the vertex functions for $Q^2 \to \infty$ by summing the asymptotically leading contributions order by order.[15]

(b) It is possible to understand, at least qualitatively in terms of the virtuality of the internal particles, why the renormalization effects and loops may not be crucial in the large-w region. To do this, we consider the "ladder" Feynman diagram whose leading contribution in the above kinematic limit is given by the time-ordered perturbation amplitude that we have computed order by order. The invariant momentum transfers to the virtual intermediate nucleon lines of the Feynman graph are of minimum magnitude in the region $w \gg 1$. For example, the (spacelike) invariant mass squared of the first virtual nucleon in Fig. 13 is

$$(E_p-\omega_1)^2-(\mathbf{P}-(1-\eta_1)\mathbf{P}+\mathbf{k}_{1\perp})^2 \approx -\frac{k_{1\perp}^2}{1-\eta_1}+\eta_1 M^2 \approx -k_{1\perp}^2 \quad \text{for } \eta_1 \ll 1. \quad (108)$$

The same result, i.e., that $M_i^2 = -k_{i\perp}^2$, can be similarly established for each internal nucleon line.

(c) The "ladder" that we have derived is not a usual t-channel ladder of the Regge models that one can associate with Pomeranchukon exchange. On the contrary, the electromagnetic currents are coupled directly to the nucleon line in Fig. 15 which corresponds to a nucleon exchange developing the ladder in the u channel. Thus this mechanism does not correspond to the physical picture discussed by Abarbanel, Goldberger, and Treiman[16] and by Harari[17] and, as recently and properly emphasized by Gross and Lewellyn Smith,[18] should not be associated with Regge-pole exchanges in the t channel.

We have seen, however, that our cutoff $k_{\perp\,\max}$ applies identically both to virtual and real particle emission and we believe that its identification with strong-interaction *data* is a crucial one. It is our view that it makes sense to look at local canonical field theory as a basis for computing physically interesting quantities and functional dependence *only* if one chooses a starting point for these calculations that bears some resemblance to the real observable world. A finite series of perturbation steps cannot and generally will not return you to a true description of physical phenomena if the starting point of these calculations is too far removed from this realm—as is the case, for example, with point coupling theories. We have attempted to avoid this difficulty in our work by introducing, by hand, a cutoff $k_{\perp\,\max}$ which corresponds to characteristic high-energy behavior. It remains for the future to verify that such a cutoff emerges theoretically as the result of a complete self-consistent dynamical calculation.

V. PREDICTIONS

We distinguish two kinds of predictions of our formalism. Predictions of the first kind follow merely from the general parton model we have derived and do not depend on the detailed dynamics of strong interactions. Predictions of the second kind follow from the specific interaction Hamiltonian assumed to describe the strong-interaction dynamics of the nucleon.

We first list a few predictions of the first kind. The first four of these, being general consequences of the scaling law for the structure functions, are already contained in Bjorken's and Feynman's work.

(i) In terms of $F_1(w)$ and $F_2(w)$ defined by (80), the differential cross section for deep-inelastic electron-nucleon scattering in the laboratory system [Eq. (2) of Paper I] becomes

$$\frac{d^2\sigma}{dw\,d\cos\theta} = \left(\frac{d\sigma}{d\cos\theta}\right)_R \left(\frac{\epsilon'}{\epsilon}\right)^2 \frac{1}{w} \times \left[F_2(w)+2\left(\frac{\nu}{M}\right)F_1(w)\tan^2(\tfrac{1}{2}\theta)\right], \quad (109)$$

where ϵ and ϵ' are the energies of the initial and final electron and θ is the electron scattering angle; and

$$\left(\frac{d\sigma}{d\cos\theta}\right)_R = \frac{8\pi\alpha^2}{(Q^2)^2}\epsilon^2\cos^2(\tfrac{1}{2}\theta) \quad (110)$$

is the differential cross section for Rutherford scattering from an infinitely heavy pointlike proton. This result shows explicitly that the existence of a Bjorken limit implies a cross section for deep-inelastic electron-nucleon scattering many orders of magnitude greater than the corresponding cross sections in the resonance regions at the same large values of Q^2. This conclusion is supported by the present SLAC and DESY data[5] which indicate that the strong dependence of the electron-proton scattering cross section which decreases roughly as $1/Q^8$ relative to the pointlike-proton value indeed disappears in the deep-inelastic region.

(ii) Experimental data are usually analyzed in terms of the cross sections σ_t and σ_l for absorption of transverse and scalar, or longitudinally polarized, virtual photons of mass $-Q^2$ on the proton.[19] These cross

[15] T. Appelquist and J. Primack, Stanford Linear Accelerator Report No. SLAC-PUB-643 (unpublished). This contains reference to all earlier studies.

[16] H. Abarbanel, M. Goldberger, and S. Treiman, Phys. Rev. Letters **22**, 1078 (1969).

[17] H. Harari, Phys. Rev. Letters **22**, 1078 (1919).

[18] D. Gross and C. Llewellyn Smith, CERN Report No. TH 1043 (unpublished). Mention of the similarity of this ladder with the "Pomeranchukon" exchange was made in Ref. 1 and is misleading.

[19] L. Hand, Phys. Rev. **129**, 1834 (1963).

sections are related to the structure functions W_1 and W_2 by

$$W_1(q^2,\nu)=\frac{\nu-Q^2/2M}{4\pi^2\alpha}\sigma_t,$$
$$\nu W_2(q^2,\nu)=\frac{1-Q^2/2M\nu}{4\pi^2\alpha}Q^2\frac{\sigma_t+\sigma_l}{1+Q^2/\nu^2}. \tag{111}$$

In the Bjorken limit, these relations become

$$F_1(w)=\frac{1}{4\pi^2\alpha}\left(1-\frac{1}{w}\right)M\nu\sigma_t,$$
$$F_2(w)=\frac{1}{4\pi^2\alpha}\left(1-\frac{1}{w}\right)Q^2(\sigma_t+\sigma_l), \tag{112}$$

and, in particular,

$$\frac{F_1(w)}{F_2(w)}=\tfrac{1}{2}w\left(\frac{\sigma_t}{\sigma_t+\sigma_l}\right). \tag{113}$$

We recall that the pion current contributes only to $F_2(w)$ and the nucleon current contributes to both structure functions with a fixed ratio given by (79a). Consequently, if the pion current, or spin-0 currents, in general, dominates, then

$$F_1(w)=0, \quad \text{or} \quad \sigma_t=0 \quad \text{(spin-0 current)}, \tag{114}$$

and if nucleon current (or spin-$\frac{1}{2}$ currents in general) dominates, then

$$\frac{F_1(w)}{F_2(w)}=\tfrac{1}{2}w, \quad \text{or } \sigma_l=0 \quad \text{(spin-}\tfrac{1}{2}\text{ current)}. \tag{115}$$

Thus measurement of the ratio σ_t versus σ_l will give clues to the constitution of the electromagnetic current. The same conclusions (114) and (115) are obtained by Callan and Gross[20] from considerations based on direct assumptions on the form of the interaction and of the current operator for the hadron.

(iii) According to (81) the weighted integral of $F_2(w)$, or νW_2, represents the weighted square of the charge in the constituents inside a physical proton—or in our model in which all charges are of unit magnitude, it is the mean number of the charged constituents inside a physical proton. If the present trend of SLAC data continues, i.e., if νW_2 falls only very slowly with increasing w or even stays flat for large w, the weighted integral (81) may even diverge. One would conclude in this event that an adequate description of the proton structure in terms of elementary constituents requires an infinite number of these particles. Thus, in contrast with nuclei which are well approximated by structures made up of weakly bound and well-separated individual nucleons, the proton will not allow such a simple description.

[20] C. Callan and D. Gross, Phys. Rev. Letters **22**, 156 (1969).

In the nuclear case of loosely bound, well-identified nucleons, the inelastic scattering cross section $d^2\sigma/d|\mathbf{q}|^2d\nu$ as a function of energy transfer ν, and for constant and large values of the 3-momentum transfer to the nucleus, $|\mathbf{q}|\geq 150$ MeV/c, shows a quasi-elastic peak at $\nu\approx|\mathbf{q}|^2/2M$. This is just the energy of recoil of a single nucleon from the nucleus, and its location tells the mass of the nuclear constituent while its width measures the momentum distribution of the nucleons bound in the nuclear ground state. The area under the inelastic scattering curve is given simply in the large-$|\mathbf{q}|$ limit—i.e., the limit in which the correlations between different nucleons are negligible and each one scatters independently and incoherently—by

$$\int_{\nu_{\min}}^{\infty}d\nu\left.\frac{d^2\sigma}{d|\mathbf{q}|^2d\nu}\right|_{|q|^2=\text{const}}=\frac{4\pi\alpha^2}{|\mathbf{q}|^4}Z. \tag{116}$$

The analogous result in the relativistic problem of deep-inelastic scattering from the proton is derived from Eq. (2) of Paper I by going to the infinite-energy limit so that $\epsilon'/\epsilon\to 1$ and $\theta\to 0$, yielding

$$\int_{\nu_{\min}}^{\infty}d\nu\left.\frac{d^2\sigma}{dQ^2d\nu}\right|_{Q^2=\text{const}}=\frac{4\pi\alpha^2}{(Q^2)^2}\int_{\nu_{\min}}^{\infty}d\nu\,W_2. \tag{117}$$

Thus we can say that in the Bjorken limit of scaling,

$$Z\to\int_{\nu_{\min}}^{\infty}d\nu\,W_2=\int_1^{\infty}\frac{dw}{w}F_2(w). \tag{118}$$

In our model of a unit-charge proton made of unit-charge constituents, we have seen in (81) and (82) that the right-hand side is greater than or equal to unity and gives the mean number of charged constituents in the proton. Were the proton, on the other hand, composed of a fixed number (say z) of charged constituents each bearing a fraction $1/z$ of the charge, plus other neutral constituents, then as (81) makes clear

$$\sum_i\lambda_{n,i}^2=\frac{z}{z^2}=\frac{1}{z}. \tag{119}$$

The $1/z$ is a finite suppression factor expressing the ratio of sum of squares of charges for incoherent scattering, z, to the square of the sum of charges, z^2, for coherent scattering. In this, z directly corresponds to Z for a nucleus with the right-hand side of (116) written as $4\pi(Z\alpha)^2|q|^2Z$.

The preliminary SLAC data suggest no such comfort for a simple nuclear-type "parton" model—at least thus far. A quasi-elastic peak is not present and the sum rule may well diverge, although thus far we can say only that

$$\int_1^{20}\frac{dw}{w}F_2(w)\approx 0.7.$$

We should not be surprised if the right-hand side does in fact diverge since, as indicated in (112), the high-ν limit of νW_2 is the same as that of the total photoabsorption cross sections for very virtual spacelike photons of mass $q^2=-Q^2\ll -M^2$. Underlying this possible difference between the right-hand side of (118) and a finite charge Z is the presence of an additional physical interaction mechanism present in high-energy processes but absent from the classical nuclear realm, and these are inelastic channels for particle production. Many new particle-production channels open up with increasing energies, leading to constant total cross sections in the high-energy limit as incident nucleons, pions, or real photons are absorbed on a black or very dark grey target hadron. Perhaps a similar behavior will characterize the cross sections for incident virtual photons of very large negative (mass)^2. The large-w or high-energy limit of our model as in Fig. 15 did not coincide with the usual picture of diffraction scattering as represented by a t-channel ladder. However, it was dominated by the inelastic scattering to multipion final states.

For this reason a literal "parton" model in terms of a fixed number of parton constituents may be inadequate. In their parton analysis, Bjorken and Paschos[4] introduced an infinite number of partons in order to generate a flat curve for νW_2 and avoid the unobserved quasi-elastic peak. In our present approach we have given the "partons" a unique interpretation—i.e., they are the series of constituents generated by the U matrix operating on the physical one-proton state—i.e., the series $|UP\rangle$ of Eqs. (57) or (72). In the present model they are just the multiparticle pion-nucleon states generated by the perturbation series.

(iv) In (79) the delta function $\delta(\eta_{n,i}-1/w)$ projects out the components in the expansion of $|UP\rangle$ with charged constituents of longitudinal momentum $(1/w)P$. Thus νW_2 or $F_2(w)$ is closely related to the longitudinal momentum distribution of the proton's constituents in an infinite-momentum frame. One should also ask, given the information about the proton structure revealed by the electron-nucleon scattering, what one can infer about purely hadronic processes, such as proton-proton scattering. The answer to this question is, however, outside the scope of our present program.

(v) As discussed in more detail in the conclusion of Paper I, our analysis shows that a picture of the proton as composed of point partons for deep-inelastic scattering is consistent with a picture of the proton as a composite charge structure with vanishing elastic form factor for asymptotically large momentum transfers. Thus the inequality (81) and the vanishing limit $F(q^2)\to 0$ as $q^2\to\infty$ can both be understood in our model if the probability of finding a bare proton in the physical proton state vanishes—i.e., $Z_2=0$ in (11).

(vi) As discussed in connection with the simplification introduced by the Bjorken limit (see Fig. 8 in particular), each scattering process produces two well-separated and identified groups of particles [(A) and (B) in Fig. 8] in the final state. In the laboratory system these two groups of particles look as follows. Particles in group (B) recoil with large total momentum along direction $\mathbf{q}$ and particles in group (A) are left behind with small total momentum.

(vii) In Paper I we showed that the crossing properties of field theory and the positivity of a physical cross section lead to a remarkable theorem for the threshold behavior of the structure function $F_2(w)$. According to this theorem, if the pion current (or spin-0 current more generally) dominates near the threshold $w\geq 1$, then

$$F_2(w)\simeq C_\pi(w-1)^{2n},\quad n=0,\,1,\,2,\,\ldots. \tag{120}$$

On the other hand, if the nucleon current (or spin-$\frac{1}{2}$ current more generally) dominates near the threshold $w\geq 1$, then

$$F_2(w)\simeq C_N(w-1)^{2n+1},\quad n=0,1,2,\ldots. \tag{121}$$

Therefore, a careful measurement of the curvature of $F_2(w)$ as a function of w near the threshold will provide interesting information about the current constitution as well as the structure of the proton.

Specific predictions based on the particular model (1) are summarized as follows.

(a) The recent SLAC data[5] indicate that $\nu W_2{}^{(p)}$ for the proton depends only weakly on w for large w and may even be approaching a constant for large w. This demands

$$\xi\sim 1,\quad \text{or}\quad k_{\perp\,\max}{}^2/M^2\sim 0.3, \tag{122}$$

which is consistent with the indication from other high-energy collision data, $k_{\perp\,\max}\approx 400\sim 500$ MeV. However, the precise equality $\xi=1$, if confirmed by further experiments at higher energies, would have to be viewed as an accident, since the ladder we have derived in Fig. 15 for the limiting behavior for large w is not the t-channel one usually associated with diffraction scattering, or the Pomeranchukon exchange.

(b) The fact that $W^{(p)}$ and $W^{(n)}$ approach each other rapidly makes it desirable to estimate the next leading contributions in $\ln w$, since the difference $W^{(p)}-W^{(n)}$ is very important in calculating the proton-neutron mass difference. Notice that the sign of $W^{(p)}-W^{(n)}$ is negative. However, since the series of $W^{(p)}-W^{(n)}$ is an alternating one leading to a sum smaller than its individual parts, we think this result is not significant. We also need these next leading contributions to evaluate c and verify that the series of leading terms yields the dominant sum.

(c) The ratio of structure functions in this limit, $W_1/\nu W_2=+w/2M$, corresponds to a vanishing of the ratio of "scalar" to "transverse" photoabsorption cross sections for virtual photons of mass Q^2 on protons. It corresponds to the Callan-Gross[20] result for a spin-$\frac{1}{2}$ quark current because, as we have seen, the current interacts with the spin-$\frac{1}{2}$ nucleon in the high-w limit. It

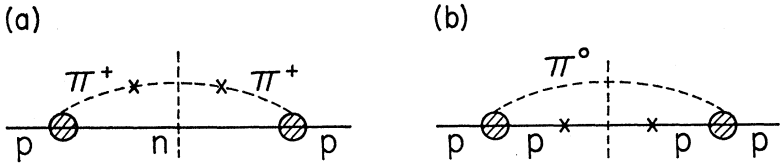

FIG. 16. Diagrams with *ad hoc* form factors inserted at the pion-nucleon vertices to dampen the amplitude when the virtual pion (a) or nucleon (b) is very virtual.

is opposite to the limit proposed by Sakurai[21] from his vector-dominance model which leads to $\sigma_l/\sigma_T \propto Q^2/m_\rho{}^2$ for large Q^2 and hence to $W_1/\nu W_2 \to 0$, corresponding to absorption on a "boson" current.

(d) The multiplicity of pions produced is given by $\bar{n}_\pi \approx \xi \ln w$. This follows from (92) and (95) if each term in the series is weighted by n, the number of pions.

(e) Our model also predicts that the pions are focused in momentum space with transverse momentum $<k_{\perp\,\max}$ about the incident-electron direction while the nucleon recoils with the large momentum $\mathbf{q}$. This is so because in the large-w region the electromagnetic current interacts only with the proton in the dominant class of diagrams.

(f) We are not able to perform a reliable calculation near $w \simeq 1$ from our field-theoretical model, since the virtual particles involved are very virtual, and the off-shell effects must be correctly taken into account. This is in contrast to our results for large $w \gg 1$, where we found the intermediate particles to be close to their energy shells and the vertex and self-energy corrections to contribute lower powers of $\ln w \gg 1$ for each order of g^2. However, a plausible conjecture can be made. Diagrams without strong vertex corrections properly included indicate that the pion current gives the dominant contribution near $w \simeq 1$. For example, to lowest order in g^2, we find near $w \geq 1$ from $F_2{}^{(18a)}$ of the Appendix for the pion current and from (89) for the nucleon-current contribution that

$$F_2(w) \cong \frac{g^2}{16\pi^2} \ln\left(1+\frac{k_{\perp\,\max}{}^2}{\mu^2}\right)(w-1) \quad \text{(nucleon current)},$$
$$F_2(w) \cong \frac{g^2}{8\pi^2} \ln\left(1+\frac{k_{\perp\,\max}{}^2}{M^2}\right) \quad \text{(pion current)}. \tag{123}$$

The virtual particle (a proton in the first case and a pion in the second) has a large (spacelike) invariant mass proportional to $k_\perp{}^2/(w-1)$. If a form factor is included at each of the two pion-nucleon vertices, as illustrated in Fig. 16, Eq. (123) becomes

$$F_2 \propto (w-1) F_p{}^2\left(\frac{C}{w-1}\right) \quad \text{(nucleon current)},$$
$$F_2 \propto F_\pi{}^2\left(\frac{C'}{w-1}\right) \quad \text{(pion current)}. \tag{124}$$

[21] J. J. Sakurai, Phys. Rev. Letters **22**, 981 (1969); C. Cho, G. Gounaris, and J. Sakurai, Phys. Rev. **186**, 1734 (1969).

The subscripts p or π at the squares of the pion-nucleon form factors indicate the particle which is virtual. If F_p and F_π behave similarly for large momentum transfers, then the pion current will continue to dominate with one less power of $(w-1)$ as $w \to 1$ when the vertex corrections are included. On the basis of our conjecture, we interpret $F_2(w)$ near $w \sim 1$ as a measure of the asymptotic pion-nucleon form factor. Available data from SLAC[5] are consistent with the fit

$$F_2(w) \approx C_1(w-1)^2, \quad w \geq 1$$

indicating that, if our conjecture that the pion current dominates in the threshold region is correct, the pion-nucleon form factor decreases with the first inverse power of the invariant momentum transfer squared, a result that we consider as reasonable.

Note added in proof. See the later discussion on this point in S. D. Drell and T. M. Yan, Phys. Rev. Letters **24**, 181 (1970).

VI. SUMMARY AND CONCLUSION

A field-theoretical derivation of the "parton model" for electron-nucleon scattering in the Bjorken limit is presented in detail in this second of a series of papers on lepton-hadron dynamics. A fundamental assumption essential to this derivation is the existence of an asymptotic region in which the momentum and energy transfers to the hadrons can be made greater than the transverse momenta of their virtual constituents or "partons" in an infinite-momentum frame. Present high-energy scattering data indicate strongly that the transverse momenta of the final particles are indeed limited in magnitude. We suppress large transverse momenta by a simple cutoff at each strong vertex. The self-consistent requirement of preserving the unitarity of the U matrix demands that the *same* cutoff be applied to both the *real* final particles and the *virtual* particles present in internal loops.

As discussed earlier, the entire role of the cutoff is to make all integrals over intermediate particle momenta finite as we let $Q^2 \to \infty$, so that we can classify leading terms in a hierarchy simply according to numbers of powers of Q^2 in the numerator minus the number in the denominator.

Its specific form is of no concern for establishing the general result that the structure functions depend on the single variable $w = 2M\nu/Q^2$.

To move beyond this general derivation of the scaling behavior and compute values for the structure functions from our field-theory model, we must further restrict

the kinematic region by taking the limit $w \gg 1$ in addition to letting Q^2 and $M\nu$ grow asymptotically large in the Bjorken limit. In this limit, the results as assembled in Eqs. (100)–(103) depend on a transverse momentum cutoff. However, as indicated by (108), the square of the transverse momentum corresponds to the negative of the invariant squared mass of the intermediate-particle masses and thus the transverse momentum cutoff has a Lorentz-invariant significance in terms of the maximum invariant mass created at the individual vertices.

We have now developed a formalism that not only leads to a "parton" model for deep-inelastic scattering but has provided the theoretical basis for accomplishing the crossing to the deep-inelastic annihilation channel as described in Paper I. This was our primary motivation in turning to a canonical field-theory framework, as we shall show in detail in the next paper of this series. This is our justification for presenting so inelegant an approach. We know of no other procedure for accomplishing the crossing and arriving at predictions for the deep-inelastic annihilation channel.

ACKNOWLEDGMENTS

We wish to acknowledge valuable conversations with colleagues at SLAC, in particular discussions with J. D. Bjorken and R. P. Feynman.

APPENDIX

In this appendix we present the explicit calculations of the structure functions in the Bjorken limit up to fourth order in the strong-interaction coupling constant g.

Results of all diagrams from nucleon-current contributions are given, but only a few examples for diagrams from pion-current contributions are listed. These results are listed here partly because they will be referred to when we study the crossing properties of the structure functions W_1 and W_2 in our next paper on electron-positron annihilation processes. In these results the initial nucleon is assumed to be a proton. For diagrams with the nucleon current contributing, all the pions are taken to be neutral. For diagrams with the pion current contributing, the pion which interacts with the current is taken to be a π^+ and the others are assumed to be neutral. Momentum labels and parametrizations are given along with these diagrams in Figs. 17 and 18. Only $F_2(w)$ is given since $F_1(w)$ is trivially obtainable by using (75) or (76). The contribution of a particular diagram, say Fig. 17(a), will be denoted by $F_2^{(17a)}$.

It suffices to say that as $w \to \infty$ none of these diagrams gives a contribution to $F_2(w)$ comparable with the contributions of the dominant class of diagrams given in (92), as can be verified easily from the explicit expressions given below. A few further remarks about these results are worth noting: (1) The contributions $F_2^{(17s_1)}$ and $F_2^{(17s_2)}$ correspond to the virtual nucleon with momentum P_1'' moving with positive and negative longitudinal momentum, respectively; $F_2^{(17t_1)}$ and $F_2^{(17t_2)}$ correspond to the virtual antinucleon with momentum $\bar{P}_1''$ moving with positive and with negative longitudinal momentum. (2) Notice that $F_2^{(17s_1)}$, $F_2^{(17s_2)}$, $F_2^{(17t_1)}$, and $F_2^{(17t_2)}$ separately diverge logarithmically at the endpoints of the η' integration. Nevertheless, the sums $F_2^{(17s_1)}+F_2^{(17t_2)}$ and $F_2^{(17s_2)}+F_2^{(17t_1)}$ are divergence free. It can be shown, by a calculation analogous to that for δM, that if a small and same cutoff is introduced for all the η' integrations, the contributions from the infinitesimal regions of η', when summed together, cancel each other. (3) As explained in Sec. IV, it is required by self-consistency that the transverse momentum cutoff for the *real* final particles be identified with the transverse momentum cutoff for the *virtual* particles appeared in the internal loops. This procedure assures the maintenance of the unitarity of the U matrix in the presence of a finite cutoff. As a result all the internal loop integrals are unambiguously well defined, since the cutoff is finite. For this reason we have not carried out the conventional renormalization program for the vertex in the present calculation. This can be done directly, if one wishes, by computing the renormalized coupling constant in terms of $k_{\perp\,\max}^2$ and unrenormalized coupling constant according to the method outlined in Sec. II. (4) In

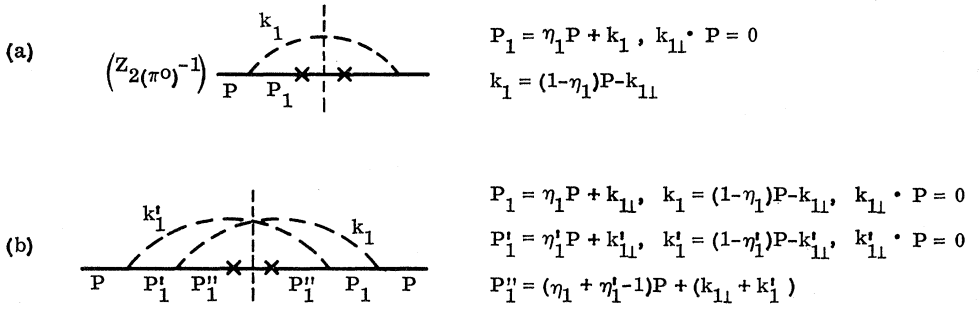

FIG. 17. Diagrams of nucleon-current contributions up to g^4. In these diagrams $Z_{2(\pi^0)}$ is given by Eq. (18), δM by Eq. (45), $\delta M_a^{(1)}$ by Eq. (33), and $\delta\mu_a^2$ by Eq. (46).

(c) 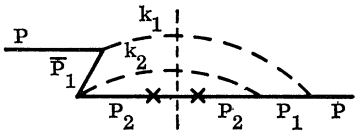

$P_1 = \eta_1 P + k_{1\perp} = -\bar{P}_1$, $k_1 = (1-\eta_1)P - k_{1\perp}$, $k_{1\perp} \cdot P = 0$

$P_2 = \eta_2 P_1 + k_{2\perp}$, $k_2 = (1-\eta_2)P_1 - k_2$, $k_{2\perp} \cdot P = 0$

(d) 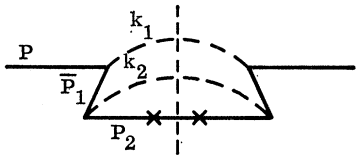

$\bar{P}_1 = -\eta_1 P - k_{1\perp} \equiv -P_1$, $k_1 = (1-\eta_1)P - k_{1\perp}$, $k_{1\perp} \cdot P = 0$

$P_2 = \eta_2 P_1 + k_{2\perp}$, $k_2 = (1-\eta_2)P_1 - k_{2\perp}$, $k_{2\perp} \cdot P_1 = 0$

(e) 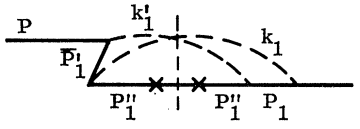

$\bar{P}'_1 = -\eta'_1 P - k'_{1\perp}$, $k'_1 = (1-\eta'_1)P - k'_{1\perp}$, $k'_{1\perp} \cdot P = 0$

$P_1 = \eta_1 P + k_{1\perp}$, $k_1 = (1-\eta_1)P - k_{1\perp}$, $k_{1\perp} \cdot P = 0$

$P''_1 = (\eta_1 + \eta'_1 - 1)P + (k_{1\perp} + k'_{1\perp})$

(f) 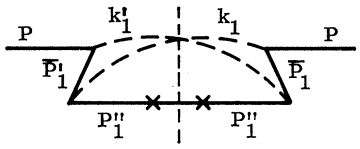

$\bar{P}_1 = -\eta_1 P - k_{1\perp}$, $k_1 = (1-\eta_1)P - k_{1\perp}$, $k_{1\perp} \cdot P = 0$

$\bar{P}'_1 = -\eta'_1 P - k'_{1\perp}$, $k'_1 = (1-\eta'_1)P - k'_{1\perp}$, $k'_{1\perp} \cdot P = 0$

$P''_1 = (\eta_1 + \eta'_1 - 1)P + (k_{1\perp} + k'_{1\perp})$

(g) 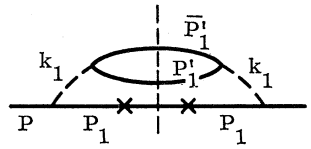

$P_1 = \eta_1 P + k_{1\perp}$, $k_1 = (1-\eta_1)P - k_{1\perp}$, $k_{1\perp} \cdot P = 0$

$P'_1 = \eta_2 k_1 + k_{2\perp}$, $P'_1 = (1-\eta_2)k_1 - k_{2\perp}$, $k_{2\perp} \cdot k_1 = 0$

(h) 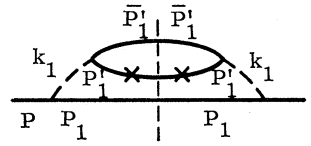

Same parametrization as in (g)

(i) 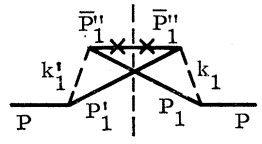

$P'_1 = \eta'_1 P + k'_{1\perp}$, $k'_1 = (1-\eta'_1)P - k'_{1\perp}$, $k'_{1\perp} \cdot P = 0$

$P_1 = \eta_1 P + k_{1\perp}$, $k_1 = (1-\eta_1)P - k_{1\perp}$, $k_{1\perp} \cdot P = 0$

$\bar{P}''_1 = (1-\eta_1-\eta'_1)P - (k_{1\perp} + k'_{1\perp})$

(j) 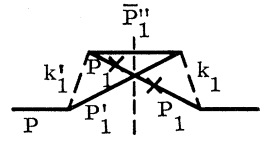

Same parametrization as in (i).

(k) 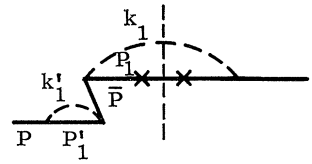

$P'_1 = \eta'_1 P + k'_{1\perp}$, $k'_1 = (1-\eta'_1)P - k'_{1\perp}$, $k'_{1\perp} \cdot P = 0$

$P_1 = \eta_1 P + k_{1\perp}$, $k_1 = (1-\eta_1)P - k_{1\perp}$, $k_{1\perp} \cdot P = 0$

$\bar{P} = -P$

(l) 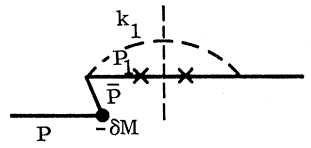

$P_1 = \eta_1 P + k_{1\perp}$, $k_1 = (1-\eta_1)P - k_{1\perp}$, $k_{1\perp} \cdot P = 0$

$\bar{P} = -P$

FIG. 17. *(Continued)*

(m) 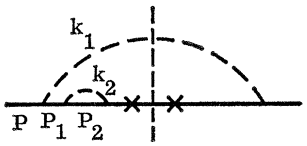

$P_1 = \eta_1 P + k_{1\perp}$, $k_1 = (1-\eta_1)P - k_{1\perp}$, $k_{1\perp} \cdot P = 0$
$P_2 = \eta_2 P_1 + k_{2\perp}$, $k_2 = (1-\eta_2)P - k_{2\perp}$, $k_{2\perp} \cdot P_1 = 0$

(n) 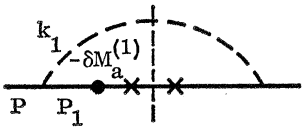

Same parametrization as in (a)

(o) 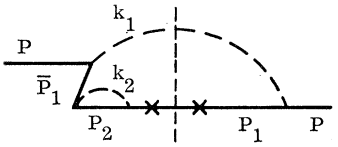

Same parametrization as in (c)

(p) 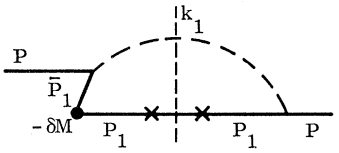

$P_1 = \eta_1 P + k_{1\perp} = -\bar{P}_1$, $k_{1\perp} = (1-\eta_1)P - k_{1\perp}$, $k_{1\perp} \cdot P = 0$

(q) 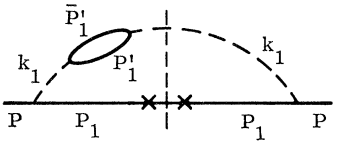

Same parametrization as in (g)

(r) 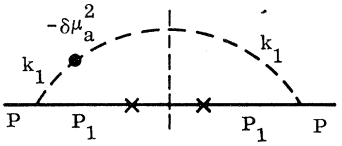

Same parametrization as in (a)

(s) 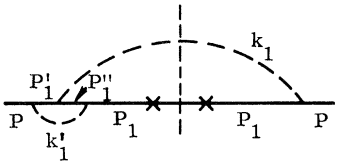

Same parametrization as in (b)

(t) 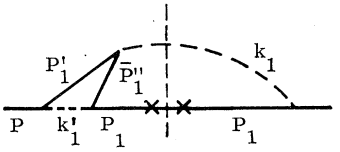

Same parametrization as in (i)

(u) 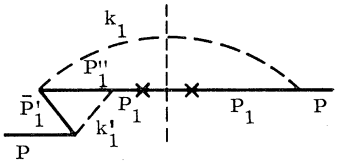

$P_1 = \eta_1 P + k_{1\perp}$, $k_1 = (1-\eta_1)P - k_{1\perp}$, $k_{1\perp} \cdot P = 0$
$\bar{P}'_1 = -\eta'_1 P - k'_{1\perp}$, $k'_1 = (1-\eta'_1)P - k'_{1\perp}$, $k'_{1\perp} \cdot P = 0$
$P''_1 = (\eta_1 + \eta'_1 - 1)\, P + (k_{1\perp} + k'_{1\perp})$

FIG. 17. (*Continued*)

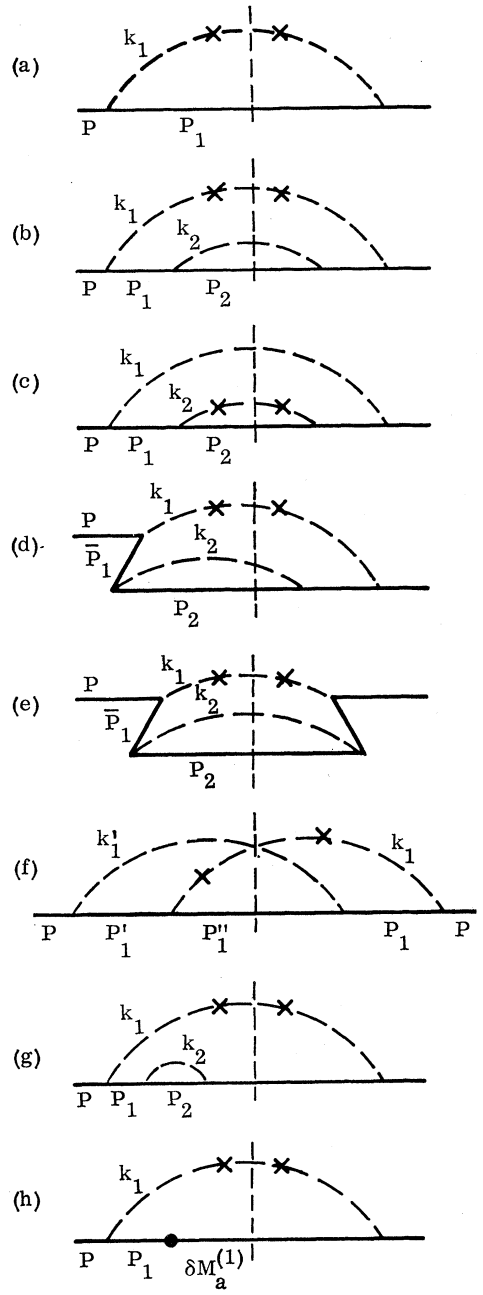

Same parametrization as in Fig. 17(a).

Same parametrization as in Fig. 17(m).

Same parametrization as in Fig. 17(m).

Same parametrization as in Fig. 17(c).

Same parametrization as in Fig. 17(d).

Same parametrization as in Fig. 17(b).

Same parametrization as in Fig. 17(m).

Same parametrization as in Fig. 17(a).

FIG. 18. Examples of second-order and fourth-order pion-current contributions. In diagram (h), $\delta M_a^{(1)}$ is given by Eq. (33).

Fig. 17(m) only the bubble in which both the nucleon and the pion have positive longitudinal momenta is included. The other bubble contributions are cancelled by the corresponding mass renormalization counter terms introduced into H_1. This explains why only $\delta M_a^{(1)}$ is retained in Fig. 17(n). The same remark applies to the nucleon-antinucleon bubbles and corresponding mass-renormalization counter terms on a pion line as in Figs. 17(q) and 17(r). (5) After symmetrical integrations in the transverse momentum, $F_2^{(17k)}$ is seen to be cancelled exactly by $F_2^{(17l)}$, with δM given by (45). This is to be expected since, in a Feynman-diagram calculation, the net effect of bubbles on an external line after removing the mass renormalization is known to be a pure wave-function renormalization. The net effect in this case is presented by $F_2^{(17a)}$. (6) The grouping of $F_2^{(17q)}$, $F_2^{(17r)}$, and $F_2^{(17g)}$ together and $F_2^{(18b)}$, $F_2^{(18g)}$, and $F_2^{(18h)}$ together is particularly useful in studying the crossing properties of the structure functions. To obtain $F_2^{(17q,r,g)}$ and $F_2^{(18b,g,h)}$, the

following identities are used:

$$\frac{2}{(E_p-E_1-E_1'-\bar{E}_1')(E_p-E_1-\omega_1)^3}-\frac{2}{(\omega_1-E_1'-\bar{E}_1')(E_p-E_1-\omega_1)^3}+\frac{1}{(E_p-E_1-E_1'-E_1')^2(E_p-E_1-\omega_1)^2}$$

$$=\frac{1}{(E_p-E_1-E_1'-\bar{E}_1')^2(\omega_1-E_1'-\bar{E}_1')^2}-\frac{1}{(E_1-E_1-\omega_1)^2(\omega_1-E_1'-\bar{E}_1')^2},$$

$$\frac{1}{(E_p-E_1-\omega_1)^2(E_p-E_2-\omega_1-\omega_2)^2}-\frac{2}{(E_p-E_1-\omega_1)^2(E_1-E_2-\omega_2)(E_1-E_2-\omega_1-\omega_2)}$$

$$=\frac{1}{(E_1-E_2-\omega_2)^2(E_p-E_2-\omega_1-\omega_2)^2}-\frac{1}{(E_p-E_1-\omega_1)^2(E_1-E_2-\omega_2)^2}.$$

$$F_2^{(17a)}=(Z_{2(\pi^0)}-1)\frac{g^2}{16\pi^2}\frac{1}{w}\left(1-\frac{1}{w}\right)\int dk_1^2\frac{k_1^2+M^2(1-1/w)^2}{[k_1^2+M^2(1-1/w)^2+\mu^2/w]^2},$$

$$F_2^{(17b)}=\left(\frac{g^2}{(2\pi)^3}\right)^2M\nu\int\frac{d^3k_1}{2\omega_1}\frac{d^3k_1'}{2\omega_1'}\delta(q^2+2P_1''\cdot q)\left(\frac{E_1''}{E_p}\right)^2$$

$$\times\frac{\mathrm{Tr}\{(M-\gamma P)(M+\gamma P_1')(M-\gamma P_1'')(M+\gamma P_1)\}}{(2E_1)(2E_1')(2E_1'')^2(E_p-E_1-\omega_1)(E_p-E_1'-\omega_1')(E_p-E_1''-\omega_1-\omega_1')^2}$$

$$=\frac{1}{2}\left(\frac{g^2}{2(2\pi)^3}\right)^2\frac{1}{w}\int d^2k_{1\perp}d^2k_{1\perp}'\int_{1/w}^1\frac{d\eta_1}{\eta_1'}\frac{\eta_1}{[k_{1\perp}^2+M^2(1-\eta_1)^2+\mu^2\eta_1][k_{1\perp}'^2+M^2(1-\eta_1')^2+\mu^2\eta_1']}$$

$$\times\frac{\left[\begin{array}{l}[k_{1\perp}'^2+M^2(1-\eta_1')^2]\{[(1-\eta_1')k_{1\perp}+\eta_1k_{1\perp}']^2+M^2(1-\eta_1')^2\}\\ \quad-[(k_{1\perp}+k_{1\perp}')^2+M^2(2-\eta_1-\eta_1')^2][(\eta_1k_{1\perp}'-\eta_1'k_{1\perp})^2+M^2(\eta_1-\eta_1')^2]\\ \quad+[k_{1\perp}^2+M^2(1-\eta_1)^2]\{[\eta_1'k_{1\perp}+(1-\eta_1)k_{1\perp}']^2+M^2(1-\eta_1)^2\}\end{array}\right]}{\left[\begin{array}{l}[(\eta_1+\eta_1'-1)/(1-\eta_1)][k_{1\perp}^2+M^2(1-\eta_1)^2+\mu^2\eta_1]+[1/(1-\eta_1')]\\ \quad\times[(k_{1\perp}(1-\eta_1')+k_{1\perp}'\eta_1)^2+M^2(1-\eta_1')^2+\mu^2\eta_1(\eta_1+\eta_1'-1)]\end{array}\right]^2}\quad(\eta_1'=1-\eta_1+1/w),$$

$$F_2^{(17c)}=\left(\frac{g^2}{(2\pi)^3}\right)^2M\nu\int\frac{d^3k_1}{2\omega_1}\frac{d^3k_2}{2\omega_2}\delta(q^2+2P_2\cdot q)\left(\frac{E_2}{E_p}\right)^2$$

$$\times\frac{\mathrm{Tr}\{(M-\gamma P)(-M+\gamma\bar{P}_1)(M-\gamma P_2)(M+\gamma P_1)\}}{(2E_1)(2\bar{E}_1)(2E_2)^2(E_p-E_1-\omega_1)(\bar{E}_1+E_2+\omega_2)(E_p-E_2-\omega_1-\omega_2)^2}$$

$$=\frac{1}{2}\left(\frac{g^2}{2(2\pi)^3}\right)^2\frac{1}{w}\int d^2k_{1\perp}d^2k_{2\perp}\int_{1/w}^1\frac{d\eta_1}{\eta_1}(1-\eta_2)$$

$$\times\frac{(k_{2\perp}+\eta_2k_{1\perp})^2+M^2(1-\eta_1\eta_2)^2-\eta_2^2[k_{1\perp}^2+M^2(1-\eta_1)^2]-[k_{2\perp}^2+M^2(1-\eta_2)^2]}{[k_{1\perp}^2+M^2(1-\eta_1)^2+\mu^2\eta_1]\{[\eta_2(1-\eta_2)/(1-\eta_1)][k_{1\perp}^2+M^2(1-\eta_1)^2+\mu^2\eta_1]+k_{2\perp}^2+M^2(1-\eta_2)^2+\mu^2\eta_2\}^2}$$
$$(\eta_2=1/\eta_1w),$$

$$F_2^{(17d)}=\left(\frac{g^2}{(2\pi)^3}\right)^2M\nu\int\frac{d^3k_1}{2\omega_1}\frac{d^3k_2}{2\omega_2}\delta(q^2+2P_2\cdot q)\left(\frac{E_2}{E_p}\right)^2\frac{\mathrm{Tr}\{(M-\gamma P)(M-\gamma\bar{P}_1)(M-\gamma P_2)(M-\gamma\bar{P}_1)\}}{(2\bar{E}_1)^2(2E_2)^2(\bar{E}_1+E_2+\omega_2)^2(E_p-E_2-\omega_1-\omega_2)^2}$$

$$=\left(\frac{g^2}{2(2\pi)^3}\right)^2\frac{1}{w^2}\int d^2k_{1\perp}d^2k_{2\perp}\int_{1/w}^1\frac{d\eta_1}{\eta_1^3}\frac{(1-\eta_2)}{1-\eta_1}$$

$$\times\frac{1}{\{[\eta_2(1-\eta_2)/(1-\eta_1)][k_{1\perp}^2+M^2(1-\eta_1)^2+\mu^2\eta_1]+k_{2\perp}^2+M^2(1-\eta_2)^2+\mu^2\eta_2\}^2}\quad(\eta_2=1/\eta_1w),$$

$$F_2^{(17e)}=\left(\frac{g^2}{(2\pi)^3}\right)^2 M\nu\int\frac{d^3k_1}{2\omega_1}\frac{d^3k_1'}{2\omega_1'}\delta(q^2+2P_1''\cdot q)\left(\frac{E_1''}{E_p}\right)^2$$
$$\times\frac{\mathrm{Tr}\{(M-\gamma P)(-M+\gamma\bar{P}_1')(M-\gamma P_1'')(M+\gamma P_1)\}}{(2E_1)(2\bar{E}_1')(2E_1'')^2(\bar{E}_1'+E_1''+\omega_1)(E_p-E_1''-\omega_1-\omega_1')^2(E_p-E_1-\omega_1)}$$
$$=(-)\tfrac{1}{2}\left(\frac{g^2}{2(2\pi)^3}\right)^2\frac{1}{w}\int d^2k_{1\perp}d^2k_{1\perp}'\int_{1/w}^1\frac{d\eta_1}{\eta_1'}\frac{\eta_1(1-\eta_1')}{k_{1\perp}^2+M^2(1-\eta_1)^2+\mu^2\eta_1}$$
$$\times\frac{\left\{\begin{array}{r}[(1-\eta_1')k_{1\perp}+\eta_1k_{1\perp}']^2+M^2(1-\eta_1')^2-\eta_1^2[(k_{1\perp}+k_{1\perp}')^2+M^2(2-\eta_1-\eta_1')^2]\\+(\eta_1+\eta_1'-1)^2[k_{1\perp}^2+M^2(1-\eta_1)^2]\end{array}\right\}}{\left\{\begin{array}{r}[(\eta_1+\eta_1'-1)(1-\eta_1')/(1-\eta_1)][k_{1\perp}^2+M^2(1-\eta_1)^2+\mu^2\eta_1]\\+[k_{1\perp}(1-\eta_1)+k_{1\perp}'\eta_1]^2+M^2(1-\eta_1')^2+\mu^2\eta_1(\eta_1+\eta_1'-1)\end{array}\right\}^2}\quad(\eta_1'=1-\eta_1+1/w),$$

$$F_2^{(17f)}=\left(\frac{g^2}{(2\pi)^3}\right)^2 M\nu\int\frac{d^3k_1}{2\omega_1}\frac{d^3k_1'}{2\omega_1'}\delta(q^2+2P_1''\cdot q)\left(\frac{E_1''}{E_p}\right)^2$$
$$\times\frac{\mathrm{Tr}\{(M-\gamma P)(-M+\gamma\bar{P}_1')(M-\gamma P_1'')(-M+\gamma\bar{P}_1')\}}{(2\bar{E}_1)(2\bar{E}_1')(\bar{E}_1'+E_1''+\omega_1)(\bar{E}_1+E_1''+\omega_1')(E_p-E_1''-\omega_1-\omega_1')^2(2E_1'')^2}$$
$$=\left(\frac{g^2}{2(2\pi)^3}\right)^2\frac{1}{w^3}\int d^2k_{1\perp}d^2k_{1\perp}'\int_{1/w}^1\frac{d\eta_1}{\eta_1'}$$
$$\times\frac{\eta_1(1-\eta_1)(1-\eta_1')}{\left\{\begin{array}{r}(1-\eta_1')(\eta_1+\eta_1'-1)[k_{1\perp}^2+M^2(1-\eta_1)^2+\mu^2\eta_1]\\+(1-\eta_1)[(k_{1\perp}(1-\eta_1')+k_{1\perp}'\eta_1)^2+M^2(1-\eta_1')^2+\mu^2\eta_1(\eta_1+\eta_1'-1)]\end{array}\right\}^2}\quad(\eta_1'=1-\eta_1+1/w),$$

$$F_2^{(17q,r,g)}=\left(\frac{g^2}{(2\pi)^3}\right)^2 M\nu\int\frac{d^3k_1}{2\omega_1}\frac{d^3P_1'}{2E_1'}\delta(q^2+2P_1\cdot q)\left(\frac{E_1}{E_p}\right)^2$$
$$\times\frac{\mathrm{Tr}\{(M+\gamma P)\gamma_5(M+\gamma P_1)\gamma_5\}\,\mathrm{Tr}\{(M+\gamma P_1')\gamma_5(-M+\gamma\bar{P}_1')\gamma_5\}}{(2\bar{E}_1')(2\omega_1)(2E_1)^2}\left\{\frac{1}{(E_p-E_1-E_1'-\bar{E}_1')(E_p-E_1-\omega_1)^3},\right.$$
$$\left.\frac{-1}{(\omega_1-E_1'-\bar{E}_1')(E_p-E_1-\omega_1)^3},\frac{1}{(E_p-E_1-E_1'-\bar{E}_1')^2(E_p-E_1-\omega_1)^2}\right\},$$

$$2F_2^{(17q)}+2F_2^{(17r)}+F_2^{(17g)}=2\left(\frac{g^2}{2(2\pi)^3}\right)^2\frac{1}{w}\left(1-\frac{1}{w}\right)\int d^2k_{1\perp}d^2k_{1\perp}'\int_0^1 d\eta_2$$
$$\times\left\{\frac{[k_{1\perp}^2+M^2(1-\eta_1)^2][k_{2\perp}^2+M^2]}{\{k_{1\perp}^2+M^2(1-\eta_1)^2+\mu^2\eta_1+\eta_1[k_{2\perp}^2+M^2-\mu^2\eta_2(1-\eta_2)]/\eta_2(1-\eta_2)\}^2[k_{2\perp}^2+M^2-\mu^2\eta_2(1-\eta_2)]^2}\right.$$
$$\left.-\frac{k_{1\perp}^2+M^2(1-\eta_1)^2}{[k_{1\perp}^2+M^2(1-\eta_1)^2+\mu^2\eta_1]^2}\frac{k_{2\perp}^2+M^2}{[k_{2\perp}^2+M^2-\mu^2\eta_2(1-\eta_2)]^2}\right\}\quad(\eta_1=1/w),$$

$$F_2^{(17h)}=\left(\frac{g^2}{(2\pi)^3}\right)^2 M\nu\int\frac{d^3P_1}{2E_1}\frac{d^3\bar{P}_1'}{2\bar{E}_1'}\delta(q^2+2P_1'\cdot q)\left(\frac{E_1'}{E_p}\right)^2\frac{\mathrm{Tr}\{(M-\gamma P)(M+\gamma P_1)\}\,\mathrm{Tr}\{(M-\gamma P_1')(-M+\gamma\bar{P}_1')\}}{(2\omega_1)^2(2E_1')^2(E_p-E_1-\omega_1)^2(E_p-E_1-E_1'-\bar{E}_1')^2}$$
$$=2\left(\frac{g^2}{2(2\pi)^3}\right)^2\frac{1}{w^2}\int d^2k_{1\perp}d^2k_{2\perp}\int_{1/w}^1\frac{d\eta_2}{\eta_2}$$
$$\times\frac{\eta_1^2(k_{2\perp}^2+M^2)[k_{1\perp}^2+M^2(1-\eta_1)^2]}{[k_{1\perp}^2+M^2(1-\eta_1)^2+\mu^2\eta_1]^2\{\eta_2(1-\eta_2)[k_{1\perp}^2+M^2(1-\eta_1)^2+\mu^2\eta_1]+\eta_1[k_{2\perp}^2+M^2-\mu^2\eta_2(1-\eta_2)]\}^2}$$
$$(\eta_1=1-1/\eta_2w),$$

$$F_2^{(17i)}=(-)\left(\frac{g^2}{(2\pi)^3}\right)^2 M\nu\int\frac{d^3k_1}{2\omega_1}\frac{d^3k_1'}{2\omega_1'}\delta(q^2+2\bar{P}_1''\cdot q)\left(\frac{\bar{E}_1''}{E_p}\right)^2$$
$$\times\frac{\mathrm{Tr}[(M-\gamma P)(M+\gamma P_1')(-M-\gamma\bar{P}_1'')(M+\gamma P_1)]}{(2E_1)(2E_1')(2\bar{E}_1'')^2(E_p-E_1-\omega_1)(E_p-E_1-E_1'-\bar{E}_1'')^2(E_p-E_1'-\omega_1')}$$
$$=(-)\tfrac{1}{2}\left(\frac{g^2}{2(2\pi)^3}\right)^2\frac{1}{w}\int d^2k_{1\perp}d^2k_{1\perp}'\int_0^{1-1/w}\frac{d\eta_1}{\eta_1}\frac{\eta_1'(1-\eta_1)^2}{[k_{1\perp}^2+M^2(1-\eta_1)^2+\mu^2\eta_1][k_{1\perp}'^2+M^2(1-\eta_1')^2+\mu^2\eta_1']}$$
$$\times\frac{\left[\begin{array}{l}[k_{1\perp}'^2+M^2(1-\eta_1')^2]\{[(1-\eta_1')k_{1\perp}+\eta_1k_{1\perp}']^2+M^2(1-\eta_1')^2\}\\ \quad-[(\eta_1k_{1\perp}'-\eta_1'k_{1\perp})^2+M^2(\eta_1-\eta_1')^2][(k_{1\perp}+k_{1\perp}')^2+M^2(2-\eta_1-\eta_1')^2]\\ \quad+[k_{1\perp}^2+M^2(1-\eta_1)^2]\{[\eta_1'k_{1\perp}+(1-\eta_1)k_{1\perp}']^2+M^2(1-\eta_1')^2\}\end{array}\right]}{\left[\begin{array}{l}[\eta_1'(1-\eta_1-\eta_1')/\eta_1][k_{1\perp}^2+M^2(1-\eta_1)^2+\mu^2\eta_1]\\ \quad+[(1-\eta_1)k_{1\perp}'+\eta_1'k_{1\perp}]^2+M^2(1-\eta_1)^2-\mu^2\eta_1'(1-\eta_1-\eta_1')\end{array}\right]^2}\quad[\eta_1'=(1-\eta_1)-1/w],$$

$$F_2^{(17j)}=(-)\left(\frac{g^2}{(2\pi)^3}\right)^2 M\nu\int\frac{d^3k_1}{2\omega_1}\frac{d^3k_1'}{2\omega_1'}\delta(q^2+2P_1\cdot q)\left(\frac{E_1}{E_p}\right)^2$$
$$\times\frac{\mathrm{Tr}\{(M-\gamma P)(M+\gamma P_1')(-M-\gamma\bar{P}_1'')(M+\gamma P_1)\}}{(2E_1')(2\bar{E}_1'')(E_p-E_1'-\omega_1')(E_p-E_1'-\bar{E}_1''-E_1)^2(2E_1)^2(E_p-E_1-\omega_1)}$$
$$=(-)\tfrac{1}{2}\left(\frac{g^3}{2(2\pi)^3}\right)^2\left(1-\frac{1}{w}\right)^2\int d^2k_{1\perp}d^2k_{1\perp}'\int_0^{1-1/w}d\eta_1'\eta_1'$$
$$\times\frac{1}{[k_{1\perp}'^2+M^2(1-\eta_1')^2+\mu^2\eta_1'][k_{1\perp}^2+M^2(1-\eta_1)^2+\mu^2\eta_1]}$$
$$\times\frac{\left[\begin{array}{l}[k_{1\perp}'^2+M^2(1-\eta_1')^2]\{[(1-\eta_1')k_{1\perp}+\eta_1k_{1\perp}']^2+M^2(1-\eta_1')^2\}\\ \quad-[(\eta_1k_{1\perp}'-\eta_1'k_{1\perp})^2+M^2(\eta_1-\eta_1')^2][(k_{1\perp}+k_{1\perp}')^2+M^2(2-\eta_1-\eta_1')^2]\\ \quad+[k_{1\perp}^2+M^2(1-\eta_1)^2]\{[\eta_1'k_{1\perp}+(1-\eta_1)k_{1\perp}']^2+M^2(1-\eta_1)^2\}\end{array}\right]}{\left[\begin{array}{l}[\eta_1'(1-\eta_1-\eta_1')/\eta_1][k_{1\perp}^2+M^2(1-\eta_1)^2+\mu^2\eta_1]\\ \quad+[(1-\eta_1)k_{1\perp}'+\eta_1'k_{1\perp}]^2+M^2(1-\eta_1)^2-\mu^2\eta_1'(1-\eta_1-\eta_1')^2\end{array}\right]}\quad(\eta_1=1/w),$$

$$F_2^{(17k)}=(-)\left(\frac{g^2}{(2\pi)^3}\right)^2 M\nu\int\frac{d^3k_1}{2\omega_1}\frac{d^3k_1'}{2\omega_1'}\delta(q^2+2P_1\cdot q)\left(\frac{E_1}{E_p}\right)^2$$
$$\times\frac{\mathrm{Tr}\{(M-\gamma P)(M+\gamma P_1')(-M-\gamma\bar{P})(M+\gamma P_1)\}}{(2E_1')(2\bar{E})(E_p-E_1'-\omega_1')(E_p-E_1-\bar{E}-E_1'-\omega_1-\omega_1')}\frac{1}{(2E_1)^2(E_p-E_1-\omega_1)^2}$$
$$=(-)\left(\frac{g^2}{2(2\pi)^3}\right)^2\frac{1}{w}\left(1-\frac{1}{w}\right)\frac{1}{2}\int d^2k_{1\perp}d^2k_{1\perp}'\int_0^1\frac{d\eta_1'}{\eta_1'}\frac{1}{[k_{1\perp}'^2+M^2(1-\eta_1')^2+\mu^2\eta_1'][k_{1\perp}^2+M^2(1-\eta_1)^2+\mu^2\eta_1]^2}$$
$$\times\{\eta_1^2[k_{1\perp}'^2+M^2(1-\eta_1')^2]-[(\eta_1k_{1\perp}'-\eta_1'k_{1\perp})^2+M^2(\eta_1-\eta_1')^2]+\eta_1'^2[k_{1\perp}^2+M^2(1-\eta_1)^2]\}\quad(\eta_1=1/w),$$

$$F_2^{(17l)}=\left(\frac{g^2}{(2\pi)^3}\right)\delta M(M\nu)\int\frac{d^3k_1}{2\omega_1}\delta(q^2+2P_1\cdot q)\left(\frac{E_1}{E_p}\right)^2\frac{\mathrm{Tr}\{(M-\gamma P)(M+\gamma\bar{P})(M+\gamma P_1)\}}{(2\bar{E})(-\bar{E}-E_1-\omega_1)(E_p-E_1-\omega_1)^2(2E_1)^2}$$
$$=\left(\frac{g^2}{2(2\pi)^3}\right)M\delta M\frac{1}{w^2}\left(1-\frac{1}{w}\right)^2\int d^2k_{1\perp}\frac{1}{[k_{1\perp}^2+M^2(1-1/w)^2+\mu^2(1/w)]^2},$$

$$F_2^{(17m)}+F_2^{(17n)}=(-)\left(\frac{g^2}{2(2\pi)^3}\right)^2\int\frac{d^3k_1}{\omega_1}\frac{d^3k_2}{\omega_2}\delta\left(\eta_1-\frac{1}{w}\right)\left(\frac{E_1}{E_p}\right)^2$$
$$\times\frac{4(M^2-P\cdot P_1)(M^2-P_1\cdot P_2)}{(2E_1)^2(E_p-E_1-\omega_1)^2(2E_1)(E_1-E_2-\omega_2)2E_2(E_p-E_2-\omega_1-\omega_2)}$$
$$=(-)\left(\frac{g^2}{2(2\pi)^3}\right)^2\frac{1}{w}\left(1-\frac{1}{w}\right)\int d^2k_{1\perp}d^2k_{2\perp}\int_0^1 d\eta_2(1-\eta_2)$$
$$\times\frac{[k_{1\perp}^2+M^2(1-\eta_1)^2][k_{2\perp}^2+M^2(1-\eta_2)^2]}{\left[\begin{array}{l}[k_{1\perp}^2+M^2(1-\eta_1)^2+\mu^2\eta_1]^2[k_{2\perp}^2+M^2(1-\eta_2)^2+\mu^2\eta_2]\\ \times\{[\eta_2(1-\eta_2)/(1-\eta_1)][k_{1\perp}^2+M^2(1-\eta_1)^2+\mu^2\eta_1]+k_{2\perp}^2+M^2(1-\eta_2)+\mu^2\eta_2\}\end{array}\right]}\quad(\eta_1=1/w),$$

$$F_2^{(17o)}=(-)\frac{1}{2}\left(\frac{g^2}{2(2\pi)^3}\right)^2\int\frac{d^3k_1}{\omega_1}\frac{d^3k_2}{\omega_2}\delta\left(\eta_1-\frac{1}{w}\right)\left(\frac{E_1}{E_p}\right)^2$$
$$\times\frac{4[(M^2-P\cdot P_1)(M^2+\bar{P}_1\cdot P_2)-(M^2-P\cdot P_2)(M^2+P_1\cdot\bar{P}_1)+(M^2+P\cdot\bar{P}_1)(M^2-P_1\cdot P_2)]}{(2E_2)(E_p-E_1-\omega_1)^2 2\bar{E}_1(E_1+E_2+\omega_2)(2E_1)^2(E_p-E_2-\omega_1-\omega_2)}$$
$$=\frac{1}{2}\left(\frac{g^2}{2(2\pi)^3}\right)^2\frac{1}{w}\left(1-\frac{1}{w}\right)\int d^2k_{1\perp}d^2k_{2\perp}\int_0^1\frac{d\eta_2}{\eta_2}$$
$$\times\frac{[(k_{2\perp}+\eta_2k_{1\perp})^2+M^2(1-\eta_1\eta_2)^2]-\eta_2^2[k_{1\perp}^2+M^2(1-\eta_1)^2]-[k_{2\perp}^2+M^2(1-\eta_2)^2]}{[k_{1\perp}^2+M^2(1-\eta_1)^2+\mu^2\eta_1]^2\{[\eta_2(1-\eta_2)/(1-\eta_1)][k_{1\perp}^2+M^2(1-\eta_1)^2+\mu^2\eta_1]+k_{2\perp}^2+M^2(1-\eta_2)^2+\mu^2\eta_2\}}$$
$$(\eta_1=1/w),$$

$$F_2^{(17p)}=\left(\frac{g^2}{(2\pi)^3}\right)\delta M(M\nu)\int\frac{d^3k_1}{2\omega_1}\delta(q^2+2P_1\cdot q)\left(\frac{E_1}{E_p}\right)^2\frac{\mathrm{Tr}\{(M+\gamma P)(M+\gamma\bar{P}_1)(M-\gamma P_1)\}}{(2\bar{E}_1)(2E_1)^2(-E_1-\bar{E}_1)(E_p-E_1-\omega_1)^2}$$
$$=-\left(\frac{g^2}{2(2\pi)^3}\right)\delta MM\frac{1}{w}\left(1-\frac{1}{w}\right)^2\int d^2k_{1\perp}\frac{1}{[k_{1\perp}^2+M^2(1-1/w)^2+\mu^2/w]^2},$$

$$F_2^{(17s)}=\left(\frac{g^2}{2(2\pi)^3}\right)^2M\nu\int\frac{d^3k_1}{\omega_1}\frac{d^3k_1'}{\omega_1'}\delta(q^2+2P_1\cdot q)\left(\frac{E_1}{E_p}\right)^2$$
$$\times\frac{\mathrm{Tr}\{(M-\gamma P)(M+\gamma P_1')(M-\gamma P_1'')(M+\gamma P_1)\}}{(2E_1')(2E_1'')(E_p-E_1'-\omega_1')(E_p-E_1''-\omega_1-\omega_1')(2E_1)^2(E_p-E_1-\omega_1)^2},$$

$$F_2^{(17s)}=F_2^{(17s_1)}+F_2^{(17s_2)},$$

$$F_2^{(17s_1)}=\frac{1}{2}\left(\frac{g^2}{2(2\pi)^3}\right)^2\frac{1}{w^2}\left(1-\frac{1}{w}\right)\int d^2k_{1\perp}d^2k_{1\perp}'\int_{1-1/w}^1 d\eta'$$
$$\times\frac{1}{\eta_1'(\eta_1+\eta_1'-1)[k_{1\perp}'^2+M^2(1-\eta_1')^2+\mu^2\eta_1'][k_{1\perp}^2+M^2(1-\eta_1)^2+\mu^2\eta_1]^2}$$
$$\times\frac{1}{\left[\begin{array}{l}[(\eta_1+\eta_1'-1)/(1-\eta_1)][k_{1\perp}^2+M^2(1-\eta_1)^2+\mu^2\eta_1]\\ +\{[k_{1\perp}(1-\eta_1')+k_{1\perp}'\eta_1]^2+M^2(1-\eta_1')^2+\mu^2\eta_1(\eta_1+\eta_1'-1)\}/(1-\eta_1')\end{array}\right]}$$
$$\times[k_{1\perp}'^2+M^2(1-\eta_1')^2]\{[(1-\eta_1')k_{1\perp}+\eta_1k_{1\perp}']^2+M^2(1-\eta_1')^2\}-[(k_{1\perp}+k_{1\perp}')^2+M^2(2-\eta_1-\eta_1')^2]$$
$$\times[(\eta_1k_{1\perp}'-\eta_1'k_{1\perp})^2+M^2(\eta_1-\eta_1')^2]+[k_{1\perp}^2+M^2(1-\eta_1)^2]\{[(1-\eta_1)k_{1\perp}'+\eta_1'k_{1\perp}]^2+M^2(1-\eta_1)^2\}$$
$$(\eta_1=1/\omega),$$

$$F_2^{(17s_2)}=\frac{1}{2}\left(\frac{g^2}{2(2\pi)^3}\right)^2\frac{1}{w}\left(1-\frac{1}{w}\right)\int d^2k_{1\perp}d^2k_{1\perp}'\int_0^{1-1/w}d\eta_1'\frac{1}{\eta_1'(1-\eta_1-\eta_1')}$$
$$\times\frac{\eta_1^2[k_{1\perp}'^2+M^2(1-\eta_1')^2]-[(\eta_1k_{1\perp}'-\eta_1'k_{1\perp})^2+M^2(\eta_1-\eta_1')^2]+\eta_1'^2[k_{1\perp}^2+M^2(1-\eta_1)^2]}{[k_{1\perp}'^2+M^2(1-\eta_1')^2+\mu^2\eta_1'][k_{1\perp}^2+M^2(1-\eta_1)^2+\mu^2\eta_1]^2}\quad(\eta_1=1/w).$$

$$F_2^{(17t)}=(-)\left(\frac{g^2}{2(2\pi)^3}\right)^2M\nu\int\frac{d^3k_1}{2\omega_1}\frac{d^3k_1'}{2\omega_1'}\delta(q^2+2P_1q)\left(\frac{E_1}{E_p}\right)^2$$
$$\times\frac{\mathrm{Tr}\{(M-\gamma P)(M+\gamma P_1')(-M-\gamma\bar{P}_1'')(M+\gamma P_1)\}}{(2E_1')(2\bar{E}_1'')(E_p-E_1'-\omega_1')(E_p-E_1'-\bar{E}_1''-E_1)(E_p-E_1-\omega_1)^2(2E_1)^2},$$

$$F_2^{(17t)}=F_2^{(17t_1)}+F_2^{(17t_2)},$$

$$F_2^{(17t_1)}=(-)\frac{1}{2}\left(\frac{g^2}{2(2\pi)^3}\right)^2\frac{1}{w}\left(1-\frac{1}{w}\right)^2\int d^2k_{1\perp}d^2k_{1\perp}'\int_0^{1-1/w}\frac{d\eta_1'}{1-\eta_1-\eta_1'}$$
$$\times\frac{1}{[k_{1\perp}'^2+M^2(1-\eta_1')^2+\mu^2\eta_1'][k_{1\perp}^2+M^2(1-\eta_1)^2+\mu^2\eta_1]^2}$$
$$\times\frac{1}{\left\{\begin{array}{r}[\eta_1'(1-\eta_1-\eta_1')/\eta_1][k_{1\perp}^2+M^2(1-\eta_1)^2+\mu^2\eta_1]\\+\{[(1-\eta_1)k_{1\perp}'+\eta_1'k_{1\perp}]^2+M^2(1-\eta_1)^2-\mu^2\eta_1'(1-\eta_1-\eta_1')\}\end{array}\right\}}$$
$$\times([k_{1\perp}'^2+M^2(1-\eta_1')^2]\{[(1-\eta_1')k_{1\perp}+\eta_1k_{1\perp}']^2+M^2(1[\eta_1'])^2\}$$
$$-[(\eta_1k_{1\perp}'-\eta_1'k_{1\perp})^2+M^2(\eta_1-\eta_1')^2][(k_{1\perp}+k_{1\perp}')^2+M^2(2-\eta_1-\eta_1')^2]$$
$$+[k_{1\perp}^2+M^2(1-\eta_1)^2]\{[\eta_1'k_{1\perp}+(1-\eta_1)k_{1\perp}']^2+M^2(1-\eta_1)^2\})\quad(\eta_1=1/w),$$

$$F_2^{(17t_2)}=(-)\frac{1}{2}\left(\frac{g^2}{2(2\pi)^3}\right)^2\frac{1}{w}\left(1-\frac{1}{w}\right)\int d^2k_{1\perp}d^2k_{1\perp}'\int_{1-1/w}^1d\eta_1'\frac{1}{\eta_1'(\eta_1+\eta_1'-1)}$$
$$\times\frac{\eta_1^2[k_{1\perp}'^2+M^2(1-\eta_1')^2]-[(\eta_1k_{1\perp}'-\eta_1'k_{1\perp})^2+M^2(\eta_1-\eta_1')^2]+\eta_1'^2[k_{1\perp}^2+M^2(1-\eta_1)^2]}{[k_{1\perp}'^2+M^2(1-\eta_1')^2+\mu^2\eta_1'][k_{1\perp}^2+M^2(1-\eta_1)^2+\mu^2\eta_1]^2}\quad(\eta_1=1/w),$$

$$F_2^{(17u)}=\left(\frac{g^2}{(2\pi)^3}\right)^2M\nu\int\frac{d^3k_1}{2\omega_1}\frac{d^3k_1'}{2\omega_1'}\delta(q^2+2P_1\cdot q)\left(\frac{E_1}{E_p}\right)^2$$
$$\times\frac{\mathrm{Tr}\{(M-\gamma P)(-M+\gamma\bar{P}_1')(M-\gamma P_1'')(M+\gamma P_1)\}}{(2\bar{E}_1')(2E_1'')(\bar{E}_1'+E_1''+\omega_1)(E_p-E_1''-\omega_1-\omega_1')(E_p-E_1-\omega_1)^2(2E_1)^2}$$
$$=(-)\frac{1}{2}\left(\frac{g^2}{2(2\pi)^3}\right)^2\frac{1}{w^2}\left(1-\frac{1}{w}\right)\int d^2k_{1\perp}d^2k_{1\perp}'\int_{1-1/w}^1d\eta_1'\frac{1}{\eta_1'(\eta_1+\eta_1'-1)}\frac{1}{[k_{1\perp}^2+M^2(1-\eta^1)^2+\mu^2\eta_1]^2}$$
$$\times\frac{\left\{\begin{array}{r}[(1-\eta_1')k_{1\perp}+\eta_1k_{1\perp}']^2+M^2(1-\eta_1')^2-\eta_1^2[(k_{1\perp}+k_{1\perp}')^2+M^2(2-\eta_1-\eta_1')^2]\\+(\eta_1+\eta_1'-1)^2[k_{1\perp}^2+M^2(1-\eta_1)^2]\end{array}\right\}}{\left\{\begin{array}{r}[(1-\eta_1')/(1-\eta_1)](\eta_1+\eta_1'-1)[k_{1\perp}^2+M^2(1-\eta_1)^2+\mu^2\eta_1]\\+[(1-\eta_1')k_{1\perp}+\eta_1k_{1\perp}']^2+M^2(1-\eta_1')^2+\mu^2\eta_1(\eta_1+\eta_1'-1)\end{array}\right\}}\quad(\eta_1=1/w),$$

$$F_2^{(18a)}=\frac{g^2}{8\pi^2}\frac{1}{w^2}\int dk_{1\perp}^2\frac{k_1^2+M^2/(w^2)}{[k_{1\perp}^2+M^2/(w^2)+\mu^2(1-1/w)]^2},$$

$$F_2^{(18b)}+2F_2^{(18g)}+2F_2^{(18h)}=\left(\frac{g^2}{(2\pi)^3}\right)^2 2M\nu\int\frac{d^3P_2}{2E_2}\frac{d^3k_2}{2\omega_2}\delta(q^2+2k_1\cdot q)\left(\frac{\omega_1}{E_p}\right)^2$$

$$\times\mathrm{Tr}\{(M-\gamma P)(M+\gamma P_1)(M-\gamma P_2)(M+\gamma P_1)\}\left\{\frac{1}{(2E_1)^2(2\omega_1)^2(E_p-E_1-\omega_1)^2(E_p-E_2-\omega_1-\omega_2)^2}\right.$$

$$\left.-\frac{2}{(2E_1)^2(2\omega_1)^2(E_p-E_1-\omega_1)^2(E_1-E_2-\omega_2)(E_p-E_2-\omega_1-\omega_2)}\right\}$$

$$=2\left(\frac{g^2}{16\pi^2}\right)^2\frac{1}{w^3}\int dk_{1\perp}^2dk_{2\perp}^2\int_0^1 d\eta_2$$

$$\times\frac{(1-\eta_2)[k_{1\perp}^2+M^2(1-\eta_1)^2][k_{2\perp}^2+M^2(1-\eta_2)^2]}{[k_{2\perp}^2+M^2(1-\eta_2)^2+\mu^2\eta_2]^2\{k_{1\perp}^2+M^2(1-\eta_1)^2+\mu^2\eta_1+[(1-\eta_1)/\eta_2(1-\eta_2)][k_{2\perp}^2+M^2(1-\eta_2)^2+\mu^2\eta_2]\}^2}$$

$$-(1-Z_{2(\pi^0)})F_2^{(17a)}\quad(\eta_1=1-1/w),$$

$$F_2^{(18c)}=\left(\frac{g^2}{(2\pi)^3}\right)^2 2M\nu\int\frac{d^3k_1}{2\omega_1}\frac{d^3P_2}{2E_2}\delta(q^2+2k_2\cdot q)\left(\frac{\omega_2}{E_p}\right)^2\frac{\mathrm{Tr}\{(M-\gamma P)(M+\gamma P_1)(M-\gamma P_2)(M+\gamma P_1)\}}{(2E_1)^2(2\omega_2)^2(E_p-E_1-\omega_1)^2(E_p-E_2-\omega_1-\omega_2)^2}$$

$$=2\left(\frac{g^2}{2(2\pi)^2}\right)^2\frac{1}{w^2}\int d^2k_{1\perp}d^2k_{2\perp}\int_{1/w}^1\frac{d\eta_1}{\eta_1}(1-\eta_1)^3$$

$$\times\frac{[k_{1\perp}^2+M^2(1-\eta_1)^2][k_{2\perp}^2+M^2(1-\eta_2)^2]}{\left\{[k_{1\perp}^2+M^2(1-\eta_1)^2+\mu^2\eta_1]\{\eta_2(1-\eta_2)[k_{1\perp}^2+M^2(1-\eta_1)^2+\mu^2\eta_1]+(1-\eta_1)[k_{2\perp}^2+M^2(1-\eta_2)^2+\mu^2\eta_2]\}^2\right\}}\quad(\eta_2=1-1/\eta_1w),$$

$$F_2^{(18d)}+F_2^{(18i)}=\left(\frac{g^2}{(2\pi)^3}\right)^2 2M\nu\int\frac{d^3P_2}{2E_2}\frac{d^3k_2}{2\omega_2}\delta(q^2+2k_1\cdot q)\left(\frac{\omega_1}{E_p}\right)^2\frac{\mathrm{Tr}\{(M-\gamma P)(-M+\gamma\bar{P}_1)(M-\gamma P_2)(M+\gamma P_1)\}}{(2E_1)(2\bar{E}_1)(2\omega_1)^2}$$

$$\times\left\{\frac{1}{(E_p-E_1-\omega_1)(\bar{E}_1+E_2+\omega_2)(E_p-E_2-\omega_1-\omega_2)^2}-\frac{1}{(E_p-E_1-\omega_1)^2(\bar{E}_1+E_2+\omega_2)(E_p-E_2-\omega_1-\omega_2)}\right\}$$

$$=\left(\frac{g^2}{2(2\pi)^3}\right)^2\frac{1}{w}\int d^2k_{1\perp}d^2k_{2\perp}\int_0^1 d\eta_2$$

$$\times\{[(k_{2\perp}+\eta_2k_{1\perp})^2+M^2(1-\eta_1\eta_2)^2]-\eta_2^2[k_{1\perp}^2+M^2(1-\eta_1)^2]-[k_{2\perp}^2+M^2(1-\eta_2)^2]\}$$

$$\times\left\{\frac{1-\eta_2}{[k_{1\perp}^2+M^2(1-\eta_1)^2+\mu^2\eta_1]\{[\eta_2(1-\eta_2)/(1-\eta_1)][k_{1\perp}^2+M^2(1-\eta_1)^2+\mu^2\eta_1]+k_{2\perp}^2+M^2(1-\eta_2)^2+\mu^2\eta_2\}^2}\right.$$

$$\left.+\frac{1-\eta_1}{\eta_2}\frac{1}{\left\{[k_{1\perp}^2+M^2(1-\eta_1)^2+\mu^2\eta_1]^2\{[\eta_2(1-\eta_2)/(1-\eta_1)]\times[k_{1\perp}^2+M^2(1-\eta_1)^2+\mu^2\eta_1]+k_{2\perp}^2+M^2(1-\eta_2)^2+\mu^2\eta_2\}\right\}}\right\}\quad(\eta_1=1-1/w),$$

$$F_2^{(18e)}=\left(\frac{g^2}{(2\pi)^3}\right)^2 4M\nu\int\frac{d^3P_2}{2E_2}\frac{d^3k_2}{2\omega_2}\delta(q^2+2k_1\cdot q)\left(\frac{\omega_1}{E_p}\right)^2\frac{4(M^2+P\cdot\bar{P}_1)(M^2+\bar{P}_1\cdot P_2)}{(2\bar{E}_1)^2(2\omega_1)^2(\bar{E}_1+E_2+\omega_2)^2(E_p-E_2-\omega_1-\omega_2)^2}$$

$$=2\left(\frac{g^2}{2(2\pi)^3}\right)^2\int d^2k_{1\perp}d^2k_{2\perp}\int_0^1 d\eta_2\frac{\eta_2^2(1-\eta_2)}{\{\eta_2(1-\eta_2)w[k_{1\perp}^2+M^2/(w^2)+\mu^2(1-1/w)]+k_{2\perp}^2+M^2(1-\eta_2)^2+\mu^2\eta_2\}^2},$$

$$F_2^{(18f)}=\left(\frac{g^2}{(2\pi)^3}\right)^2 2M\nu\int\frac{d^3P_1''}{2E_1''}\frac{d^3k_1'}{2\omega_1'}\delta(q^2+2k_1\cdot q)\left(\frac{\omega_1}{E_p}\right)^2$$

$$\times\frac{\mathrm{Tr}\{(M-\gamma P)(M+\gamma P_1')(M-\gamma P_1'')(M+\gamma P_1)\}}{(2E_1)(2E_1')(2\omega_1)^2(E_p-E_1'-\omega_1')(E_p-E_1-\omega_1)(E_p-E_1''-\omega_1-\omega_1')^2}$$

$$=\left(\frac{g^2}{2(2\pi)^3}\right)^2\frac{1}{w}\left(1-\frac{1}{w}\right)\int d^2k_{1\perp}d^2k_{1\perp}'\int_{1/w}^1\frac{d\eta_1'}{\eta_1'}\frac{1}{[k_{1\perp}^2+M^2(1-\eta_1)^2+\mu^2\eta_1][k_{1\perp}'^2+M^2(1-\eta_1')^2+\mu^2\eta_1']}$$

$$\times\frac{\left\{\begin{array}{l}[k_{1\perp}'^2+M^2(1-\eta_1')^2][(k_{1\perp}(1-\eta_1')+k_{1\perp}'\eta_1)^2+M^2(1-\eta_1')^2]\\ \quad-[(k_{1\perp}+k_{1\perp}')^2+M^2(2-\eta_1-\eta_1')^2][(\eta_1k_{1\perp}'-\eta_1'k_{1\perp})^2+M^2(\eta_1-\eta_1')^2]\\ \quad+[k_{1\perp}^2+M^2(1-\eta_1)^2][(\eta_1'k_{1\perp}+(1-\eta_1)k_{1\perp}')^2+M^2(1-\eta_1)^2]\end{array}\right\}}{\left\{\begin{array}{l}[(\eta_1+\eta_1'-1)/(1-\eta_1)][k_{1\perp}^2+M^2(1-\eta_1)^2+\mu^2\eta_1]\\ \quad+[1/(1-\eta_1')][(k_{1\perp}(1-\eta_1')+k_{1\perp}'\eta_1)^2+M^2(1-\eta_1')^2+\mu^2\eta_1(\eta_1+\eta_1'-1)]\end{array}\right\}^2}\quad(\eta_1'=1-\eta_1+1/w).$$